Targeting transcriptional coregulator OCA-B/Pou2af1 blocks activated autoreactive T cells in the pancreas and type-1 diabetes

Heejoo Kim[1,2,#], Jelena Perovanovic[1,2], Arvind Shakya[1,$], Zuolian Shen[1,2], Cody N. German[1], Andrea Ibarra[1,2], Jillian L. Jafek[1,2], Nai-Pin Lin[3], Brian D. Evavold[1], Danny H.-C. Chou[3,¶], Peter E. Jensen[1], Xiao He[1], and Dean Tantin[1,2]

[1]Department of Pathology, University of Utah School of Medicine, Salt Lake City, UT 84112, U.S.A.
[2]Huntsman Cancer Institute, University of Utah School of Medicine, Salt Lake City, UT 84112, U.S.A.
[3]Department of Biochemistry, University of Utah School of Medicine, Salt Lake City, UT 84112, U.S.A.
[#]Current address: Johnson & Johnson Research and Development, San Diego, CA 92121
[$]Current address: Bristol Myers Squibb, San Diego, CA 92121
[¶]Current address: Department of Pediatrics, Division of Endocrinology and Diabetes, Stanford University School of Medicine, Palo Alto, CA 94305

Correspondence to: Dean Tantin: dean.tantin@path.utah.edu

Summary: Kim et al. show that loss or inhibition of OCA-B in T cells protects mice from type-1 diabetes.

Abbreviations: AR, androgen receptor; DIEA, N,N-diisopropylethylamine; DCM, dichloromethane; DMF, dimethylformamide; HATU, 1-[Bis(dimethylamino)methylene]-1H-1,2,3-triazolo[4,5-b]pyridinium 3-oxid hexafluorophosphate; ICOS, Inducible T-cell costimulator; IGRP, islet-specific glucose-6-phosphatase catalytic subunit related protein; NOD, non-obese diabetic; PLNs, pancreatic lymph nodes; PMA, phorbol 12-myristate 13-acetate; RIP-mOVA, rat insulin promoter-membranous ovalbumin; scRNAseq, single-cell RNA sequencing; T1D, Type-1 diabetes; TFA, trifluoroacetic acid; TIS, triisopropylsilane; Treg, regulatory T cell; UMAP, uniform manifold approximation and projection.

Running title: OCA-B in T1D

Abstract

The transcriptional coregulator OCA-B promotes expression of T cell target genes in cases of repeated antigen exposure, a necessary feature of autoimmunity. We hypothesized that T cell-specific OCA-B deletion and pharmacologic OCA-B inhibition would protect mice from autoimmune diabetes. We developed an *Ocab* conditional allele and backcrossed it onto a diabetes-prone NOD/ShiLtJ strain background. T cell-specific OCA-B loss protected mice from spontaneous disease. Protection was associated with large reductions in islet CD8$^+$ T cell receptor specificities associated with diabetes pathogenesis. CD4$^+$ clones associated with diabetes were present, but associated with anergic phenotypes. The protective effect of OCA-B loss was recapitulated using autoantigen-specific NY8.3 mice, but diminished in monoclonal models specific to artificial or neoantigens. Rationally-designed membrane-penetrating OCA-B peptide inhibitors normalized glucose levels, and reduced T cell infiltration and proinflammatory cytokine expression in newly-diabetic NOD mice. Together, the results indicate that OCA-B is a potent autoimmune regulator and a promising target for pharmacologic inhibition.

Keywords

OCA-B, *Pou2af1*, Type-1 Diabetes, T lymphocytes, single-cell RNAseq

~40-word summary statement for the online JEM table of contents and alerts (word count: 44)

Kim and colleagues show that OCA-B in T cells is essential for the generation of type-1 diabetes. OCA-B loss leaves the pancreatic lymph nodes largely undisturbed, but associates autoreactive CD4$^+$ T cells in the pancreas with anergy while deleting potentially autoreactive CD8$^+$ T cells.

56 **Introduction**

57 Type-1 diabetes (T1D) is an autoimmune disease in which the host immune system is directed towards
58 antigens associated with pancreatic beta cells (Cooke and Plotnick, 2008; Lernmark and Larsson,
59 2013). Pathologically, T1D is characterized by insulitis, beta cell destruction and inability to produce
60 insulin. The main treatment for T1D, life-long insulin therapy, treats symptoms but not cause. The
61 development of new T1D treatments is limited by an incomplete understanding of disease mechanisms
62 (Staeva et al., 2013). Beta cell regeneration is a promising line of therapy, but still requires methods to
63 specifically block T1D autoimmunity. An ideal therapy would block autoimmunity early in the disease
64 course to spare remaining beta cell function while preserving normal immune function.

65 OCA-B, also known as Bob.1/OBF-1 (gene symbol *Pou2af1*), is a transcriptional coregulatory
66 protein named for its strong expression in the B cell lineage, where it is dispensable until after B cell
67 activation. Following B cell activation, it is essential for the generation of germinal centers (Shi et al.,
68 2015). In $CD4^+$ T cells, OCA-B docks with the transcription factor Oct1 to regulate a set of ~150 target
69 genes, including *Il2*, *Ifng* and *Csf2* (*Gmcsf*) (Shakya et al., 2015). Upon T cell activation, many of
70 these targets are activated by pathways that converge on transcription factors such as NF-AT, AP-1
71 and NF-κB. Factors like NF-AT can be thought of as the primary on/off switches for these genes, and
72 drugs that block their activity effectively block target gene expression. Such drugs have utility in many
73 contexts, but also have drawbacks including global dampening of immune function and side effects
74 due to expression in other tissues. In contrast, Oct1 and OCA-B insulate silent but previously activated
75 target genes against stable repression. Loss of either protein does not affect $CD4^+$ T cell responses to
76 stimulation in vitro or primary infection in mice (Kim et al., 2019; Shakya et al., 2015), but causes
77 target gene expression defects upon secondary stimulation in vitro (Shakya et al., 2015; Shakya et al.,
78 2011). Loss of either protein also results in defective $CD4^+$ memory T cell formation and recall
79 responses in vivo (Shakya et al., 2015). In addition, OCA-B expression is largely confined to
80 lymphocytes. OCA-B is undetectable in thymocytes and naïve $CD4^+$ T cells, but becomes stably
81 expressed after antigen stimulation (Shakya et al., 2015). Once expressed, OCA-B recruits the histone
82 lysine demethylase Jmjd1a/Jhdm2a/Kdm3a to Oct1 at target loci, where it locally removes inhibitory
83 H3K9me2 chromatin marks that would otherwise promote repressive chromatin environments (Shakya
84 et al., 2015). OCA-B also potentiates polarization of activated helper T cells towards the Th17
85 phenotype, among the most pro-inflammatory helper T cell subsets (Yosef et al., 2013).

86 Persistent antigen exposure is a common property of autoimmune responses. Among profiled
87 $CD4^+$ T cell subsets, OCA-B levels are elevated in both central memory cells and pancreas-infiltrating,

88 islet-reactive CD4$^+$ T cells (Heng et al., 2008). Both Oct1 and OCA-B are highly conserved from mice
89 to humans, and genome-wide association studies identify Oct1/OCA-B binding site polymorphisms
90 that confer predisposition to a variety of human autoimmune diseases including T1D, multiple
91 sclerosis, lupus, inflammatory bowel disease and rheumatoid arthritis (Cunninghame Graham et al.,
92 2006; Farh et al., 2015; Kiesler et al., 2009; Leon Rodriguez et al., 2016; Maurano et al., 2012; van
93 Heel et al., 2002; Vince et al., 2016). Other studies implicate polymorphisms at the *Ocab* (*Pou2af1*)
94 locus itself in different forms of autoimmunity (Games Collaborative et al., 2006; Nakamura et al.,
95 2012). We therefore hypothesized that targeting OCA-B would inhibit autoreactive, diabetogenic T
96 cell responses.

97 Here, we generate a T cell conditional mouse model of OCA-B deficiency. We show that
98 OCA-B ablation protects animals from spontaneous, polyclonal T1D. Protection was associated with
99 reduced autoreactivity of autoantigen-specific CD8$^+$ T cells in the pancreatic lymph nodes (PLNs),
100 reduced representation of these same TCR clones in the pancreatic islets and the induction of anergy in
101 potentially autoreactive islet CD4$^+$ T cell clones. The protection associated with OCA-B loss varied
102 among different TCR transgenic and monoclonal antigen models, and was weakest using synthetic
103 antigens and monoclonal transplant models. Protection was stronger using a spontaneous autoantigen-
104 specific TCR transgenic model. Using a rational-design approach, we developed membrane-
105 penetrating OCA-B peptide inhibitors that are efficacious in vitro and in mice. Collectively, the results
106 show that OCA-B is a potent and pharmacologically accessible autoimmune regulator.

107 **Results**

108 **Generation of an *Ocab* conditional allele and NOD backcrossing**

109 We generated a conditional *Ocab* (*Pou2af1*) mouse allele using embryonic stem cells provided by the
110 knockout mouse project (KOMP) repository. Deletion of the *LoxP* sites creates a null allele by
111 removing the first three exons (Fig. S1A). Breeding chimeric mice resulted in germline transmission
112 and a founder mouse (Fig. S1B, lane 2) that was crossed to a FLP deleter mouse strain (FLP^{Rosa26}) to
113 remove the reporter cassette and create a floxed conditional allele (Fig. S1A and B, lane 3).
114 Intercrossing these mice generated *fl/fl* homozygotes (Fig. S1B, lane 4) which were crossed to a
115 germline Cre deleter strain (Cre^{Rosa26}) to generate germline null (*Δ*) alleles (lanes 5 and 6). As
116 expected, homozygous *fl/fl* mice produce normal amounts of both p34 and p35 OCA-B protein
117 isoforms (Fig. S1C, lane 6), while no protein of either isoform is present in *Δ/Δ* spleens (lanes 7-8).
118 These results indicate that the *fl* allele is OCA-B sufficient and the Cre-deleted allele is a null. Crossing
119 the *fl* allele onto a CD4-cre driver, which deletes in both CD4 and CD8 compartments, resulted in
120 efficient deletion in splenic T cells (Fig. S1D). This allele therefore represents a robust system in
121 which to study OCA-B function in T cells.

122 The conditional allele was generated on a C57BL/6 background. To test the role of OCA-B
123 expression in T cells in T1D emergence, we conducted congenic backcrosses to the NOD strain
124 background. This method allows spontaneous diabetes to be produced rapidly by screening and
125 selectively breeding mice with 13 microsatellite and SNP markers associated with autoimmunity
126 (Serreze et al., 1996). *Ocab* is located on mouse chromosome 9 and distant from any of the *Idd* loci.
127 Following these markers with specific primer-pairs (Table S1), we produced backcrossed animals with
128 all 13 markers (Fig. S1E) that recapitulate spontaneous autoimmunity (not shown). For example, *Idd1*,
129 which maps to the MHC region (Hattori et al., 1986), converted to the homozygous NOD allele after 2
130 backcross generations (Fig. S1E, lane 3), whereas *Idd13*, which maps near beta-2-microglobulin
131 (Serreze et al., 1998) became NOD homozygous after 4 generations (lane 4). Genotyping identified
132 this fourth-generation backcrossed animal as having all 13 microsatellite markers and the *Ocab*
133 conditional allele (Fig. S1F, #122). This founder animal was crossed to NOD.CD4-cre in order to
134 delete OCA-B in T cells. Similar NOD backcrosses, conducted using *Ocab* null mice (Kim et al.,
135 1996), resulted in OCA-B germline-deficient NOD mice (not shown). As with the original C57BL/6
136 OCA-B germline knockout (Kim et al., 1996), all alleles were viable and fertile with no obvious health
137 issues.

138

139 **Normal baseline T cell Status in NOD mice lacking OCA-B**

140 To study the effects of T cell-specific OCA-B loss on T cell function, we performed single-cell RNA
141 sequencing (scRNAseq) and TCR clonotype analysis using $CD3^+$ T cells isolated from PLNs of
142 prediabetic 8 wk-old female NOD.*Ocab*$^{fl/fl}$CD4-cre or NOD.*Ocab*$^{fl/fl}$ littermate controls. For each
143 group, cells from 3 animals were combined for microfluidics, sequencing and analysis. ~6000
144 knockout and ~3000 control cells were identified in this analysis, most of which comprise naïve $CD4^+$
145 and $CD8^+$ cells (Fig. S2A, pink and orange), and regulatory T cells (Tregs, green). There was also a
146 small population of activated $CD4^+$+$CD8^+$ cells (blue-green), presumably in the process of exiting the
147 lymph nodes. Other than a small decrease in the percentage of activated T cells (4.4 vs 6.1%), few
148 differences in relative abundance of the populations were observed. None of the populations expressed
149 measurable amounts of *Ocab* (*Pou2af1*) mRNA (not shown), however *Pou2af1* is expressed at low
150 levels in T cells making it difficult capture by scRNAseq. In addition, few changes in gene expression
151 were identified (Fig. S2B, Table S2). We also determined TCR repertoires, identifying few changes
152 across all populations (Fig. S2C). However, specific sub-populations did show changes in TCR
153 utilization. For example, >90% of NOD $CD8^+$ T cells that display reactivity to islet-specific glucose-6-
154 phosphatase catalytic subunit related protein (IGRP) residues 206-214 express *Trbv13-3* (Vβ8.1)
155 (Wong et al., 2006). Although this clone was unchanged across the entire population of T cells (Fig.
156 S2C), it was over-represented in the effector $CD8^+$ population (Fig. S2D). In contrast, other TCR
157 clonotypes such as *Trbv13-1*, *Trbv13-2*, *Trbv1* and *Trbv15* were unchanged (not shown).
158

159 **NOD mice lacking OCA-B are protected from T1D**

160 T1D onset in NOD mice is spontaneous and acute (Makino et al., 1985). To test the impact of OCA-B
161 loss in T cells on spontaneous T1D, we compared incidence in in female NOD.*Ocab*$^{fl/fl}$CD4-cre mice,
162 and littermate controls lacking CD4-cre. Glucose was monitored 2-3 times/wk. Approximately 60% of
163 *Ocab*$^{fl/fl}$ control mice manifested spontaneous diabetes by 24 weeks of age, reaching an average of
164 >300 mg/dL by 24 weeks, while no *Ocab*$^{fl/fl}$CD4-cre mice became diabetic (Fig. 1A,B). Similar results
165 were observed using female whole-body knockout NOD.*Ocab*$^{-/-}$ compared to *Ocab*$^{+/+}$ littermate
166 controls. While ~80% of control females developed T1D within 24 weeks after birth, only ~20% of
167 NOD.*Ocab*$^{\Delta/\Delta}$ females did so (Fig. 1C). The differences in T1D penetration are likely attributable to
168 differences in the NOD backcrosses, as the 13 *Idd* NOD determinants largely but not completely
169 dictate the autoimmune phenotype. Cumulatively, the results show that OCA-B expression in T cells is
170 critical for T1D pathogenesis in NOD mice.

171 We sacrificed *Ocab*$^{fl/fl}$CD4-cre female mice and controls at 24 weeks, and determined immune
172 cell frequencies in the pancreata. We observed more T cells in the pancreata of OCA-B deficient mice
173 (not shown). An relative increase in infiltrating T cells in endpoint knockouts at endpoint is
174 understandable because the controls have annihilated their pool of beta cells and associated antigens.
175 We also studied pancreatic macrophages in these mice. Islet infiltration of F4/80^{+}CD11b^{+} macrophages
176 is critical for NOD T1D pathogenesis both in spontaneous and adoptive transfer T1D models (Peterson
177 et al., 1998; Rosmalen et al., 2000). CCL1 expressed in diabetogenic CD4^{+} T cells recruits CCR8-
178 expressing macrophages (Cantor and Haskins, 2007). OCA-B deletion decreases *Ccl1* mRNA
179 expression in stimulated, rested and re-stimulated CD4^{+} T cells compared to controls (Table S3).
180 Despite the presence of antigen greater numbers of T cells, we observed fewer macrophages in 24 wk
181 NOD.*Ocab*$^{fl/fl}$CD4-cre islets (Fig. 1D,E). In contrast, macrophages were unaffected by T cell-specific
182 OCA-B loss in prediabetic (8 wk) mice (Fig. 1D).
183 IFNγ is a direct OCA-B target gene (Shakya et al., 2015). Serum and pancreatic IFNγ levels
184 gradually rise in young NOD mice, reaching maximum at diabetes onset (Schloot et al., 2002).
185 Diabetogenic CD4^{+} and CD8^{+} T cells express IFNγ both in humans and NOD mice (Krishnamurthy et
186 al., 2008; Newby et al., 2017; Wang et al., 1997). We therefore predicted that OCA-B loss would
187 reduce IFNγ expression in islet CD4^{+} and CD8^{+} T cells. We compared IFNγ-expressing pancreatic
188 CD4^{+} and CD8^{+} T cells in female NOD.*Ocab*$^{fl/fl}$CD4-cre to littermate control mice lacking CD4-cre. In
189 12 wk prediabetic mice, CD8^{+} T cell frequencies were only slightly decreased (Fig. 1F). CD4^{+} T cells
190 at the same timepoint were also unchanged (not shown). At the time of diabetes onset (16 wk), fewer
191 IFNγ-expressing CD8^{+} T cells were present in *Ocab* conditional-deleted mice compared to controls
192 (Fig. 1G).
193
194 **T cell-specific OCA-B deletion alters the islet-infiltrating TCR repertoire**
195 We performed scRNAseq and TCR clonotype analysis similar to Fig. S2, but using older (12 wk)
196 prediabetic NOD.*Ocab*$^{fl/fl}$CD4-cre or NOD.*Ocab*$^{fl/fl}$ littermate control female mice, and using total
197 CD45^{+} cells isolated from pancreatic islets. Cells were isolated from 4 animals/group and combined for
198 microfluidics and sequencing. After filtering, ~6200 knockout and ~3800 control cells were identified.
199 Overlaying cells from both genotypes, we used their gene expression profiles to definitively identify
200 cell lineages, including naïve T cells, memory/effector CD4^{+} T cells, memory/effector CD8^{+} T cells, B
201 cells, macrophages and neutrophils (Fig. 2A). Among the different populations, the biggest relative
202 change was neutrophils, which decreased from 3.4 to 1.4% in conditional knockout islets (Fig. 2A). B

203 cells were also decreased, albeit more slightly. These changes were accompanied by increased
204 percentages of naïve T cells (32 vs. 25%). Prediabetic islets also showed significant changes in gene
205 expression between the 2 groups (Fig. 2B), the strongest of which occurred in neutrophils (e.g., *Cxcl2*,
206 down), memory/effector $CD8^+$ T cells (*Ccl4*, *Tcrg-v1*, *Itga*, down; *Tcrbv1*, *Trav8n-2*, up), NK T cells
207 (*Klra2*, *Lars2*, down) and γδT cells (*Gzma*, *Gzmb*, *Ccl5*, down).
208 We also profiled TCR utilization in pancreatic T cells. Across total T cells, few changes were
209 observed (Fig. S3), however this was largely do to similar representation in the naïve T cell pool.
210 Isolating antigen-experienced $CD4^+$ and $CD8^+$ effector + memory subpopulations revealed sharp
211 differences. For example, >90% of diabetogenic $CD8^+$ T cells displaying reactivity to $IGRP_{206-214}$
212 express *Trbv13-3* (Vβ8.1) (Wong et al., 2006). Relative to controls, this clonotype was under-
213 represented in OCA-B deficient effector + memory $CD8^+$ cells (Fig. 2C, 20.9% vs 8.6%). Based on
214 this information, we repeated the clonotype analysis, but only using the effector + memory $CD8^+$ T cell
215 cluster. Within this population, dominant TCR clonotypes were strikingly different (Fig. 2D).
216 Clonotype 1 for example is the most abundant, and corresponds to a TCRα V8N-2 chain paired with
217 TCRβ V1 or V15. It has not been associated with T1D. This clonotype was absent in control islets but
218 represented >4% of OCA-B deficient islet $CD8^+$ effector + memory T cells (Fig. 2D). Clonotype 1
219 cells overlaid with both genotypes is shown in Fig. 2E. Clonotype 2 by contrast expresses the T1D-
220 associated Vβ8.1 TCR β chain. This clonotype was strongly represented in controls (>3%) but absent
221 from OCA-B deficient effector + memory $CD8^+$ cells (Fig. 2D). In contrast to CD8, CD4-dominant
222 TCR clonotypes associated with T1D were still present in knockouts, but associated with markers of
223 anergy. For example, clonotype 4 (*Trav13-1/16N+Trbv15*) is associated with pro-diabetogenic, BDC-
224 reactive $CD4^+$ T cells (Li et al., 2009). This clonotype was enriched in the OCA-B deficient effector +
225 memory $CD4^+$ cells, but only in a CTLA4- and FR4-expressing sub-population (Fig. 2E).
226 Cumulatively, these results show that OCA-B loss from T cells significantly skews the TCR landscape
227 of islet effector/memory-like T cells to an anti-diabetogenic phenotype.
228
229 **Autoantigen-specific CD8+ T cells are present in PLNs of OCA-B deficient mice, but show**
230 **reduced reactivity and islet penetration**
231 In order to understand the basis for the reduction in autoantigen-specific $CD8^+$ T cell islet clones, we
232 studied Vβ8.1 expression and $IGRP_{206-214}$ reactivity in matched pancreatic islets and PLNs from 12 wk
233 prediabetic female *Ocab*$^{fl/fl}$CD4-cre mice or littermate *Ocab*$^{fl/fl}$ controls. Islet $CD8^+$ T cells showed
234 decreased Vβ8.1 usage (Fig. 3A), while PLNs from the same animals showed a corresponding increase

235 (Fig. 3B). To directly test diabetogenic, antigen-specific islet $CD8^+$ T cells, we used $IGRP_{206-214}$ H-$2K^d$
236 class I tetramers, which recognize TCRs expressing Vβ8.1. Islet $CD8^+V\beta8.1^+$ T cells showed a strong
237 decrease in $IGRP_{206-214}$ specificity (Fig. 3C).
238 The decrease in autoantigen-specific islet $CD8^+$ T cells and corresponding increase in the PLNs
239 in OCA-B T cell deficient mice raised two possibilities: cells in the PLNs could fail to become
240 activated, or could become activated but fail to migrate to the pancreas. In the first case, more antigen-
241 reactive cells would be observed while in the second there would be fewer. To distinguish between
242 these possibilities, we performed peptide stimulation experiments using 7 different known
243 diabetogenic self-peptides. We used 5 IGRP peptides, including $IGRP_{206-214}$ which corresponds to the
244 tetramer used above and the NY8.3 TCR transgenic mice used below. We also used two GAD65
245 epitopes, 206-214 and 546-554. 5 of the 7 peptides showed significant reductions in autoreactivity,
246 including $IGRP_{206-214}$ (Fig. 3D,E). These results indicate that potentially autoreactive cells fail to
247 become activated in the PLNs of OCA-B deficient mice.
248
249 **Protection conferred by OCA-B loss is model-specific**
250 T1D in NOD mice originates from defective negative selection in developing T cells, resulting in T
251 cell autoreactivity. OCA-B is not expressed in thymocytes and OCA-B loss does not appear to affect T
252 cell development (Shakya et al., 2015). Therefore, the protective effect of OCA-B loss in T cells likely
253 arises from blunting pre-existing autoreactivity in the periphery. To test the hypothesis that OCA-B
254 loss confers protection in simplified systems, we crossed OCA-B deficient mouse models employing
255 TCR transgenes and model antigens.
256 We crossed the germline null *Ocab* allele to BDC2.5 mice (Katz et al., 1993), which expresses
257 a CD4-restricted TCR specific for a hybrid insulin-chromogranin A peptide (Delong et al., 2016).
258 Transferring Treg-depleted T cells from BDC2.5 TCR transgenic mice into NOD.Scid mice results in
259 disease after approximately 10 d (Berry and Waldner, 2013; Presa et al., 2015). We transferred
260 $CD4^+CD25^-$ T cells from germline $Ocab^{-/-}$ or $Ocab^{+/+}$ BDC2.5 mice into NOD.Scid recipients,
261 monitoring diabetes emergence. Transplants from both $Ocab^{-/-}$ and control NOD.BDC2.5 mice resulted
262 in equivalent disease kinetics (Fig. 4A) and severity (not shown). Transferring $Ocab^{-/-}$ or control
263 NOD.BDC2.5 $CD4^+CD62L^+V\beta4^+$ T cells into NOD.Scid recipients, or total $CD4^+$ T cells into NCG
264 recipients, also resulted in equivalent disease (Fig. S4A, Fig. 4B).
265 We also tested the effect of T cell conditional OCA-B deletion in a different strain background,
266 C57BL/6J, using the artificial membranous chicken ovalbumin antigen expressed from the rat insulin

267 promoter (RIP-mOVA) (Van Belle et al., 2009). Wild-type OVA-reactive $CD8^+$ OT-I T cells were
268 transferred into either *Ocab*$^{fl/fl}$CD4-cre or control *Ocab*$^{fl/fl}$ RIP-mOVA mice. In this model, host $CD4^+$
269 T cells help transferred OT-I T cells promote T1D pathogenesis (Kurts et al., 1997). Mice were
270 infected with Lm-OVA to induce strong and synchronous beta cell destruction and loss of glucose
271 control (>400 mg/dL). No differences were observed using host mice with or without OCA-B T cell
272 deletion (Fig. S4B). These results indicate that OCA-B does not act analogously to transcription factors
273 that regulate many of the same genes, such as NF-AT. Knockouts of these factors would result in
274 broad immunosuppression and protection from T1D across models. Rather, our results suggest that
275 OCA-B loss selectively blunts immune activation in contexts such as autoantigen recognition. To test
276 this supposition and rule out the possibility that T cell transfer itself does not blunt the effect of OCA-
277 B loss, we transferred total splenocytes from polyclonal NOD.*Ocab*$^{fl/fl}$CD4-cre mice or controls. This
278 model, which takes weeks rather than days to develop T1D, recapitulates robust T1D protection with T
279 cell-specific OCA-B loss (Fig. 4C). Protection was associated with fewer IFNγ-expressing islet
280 cytotoxic T cells (Fig. 4D), and reduced insulitis in pancreatic histological sections (Fig. 4E,F).
281 Because the Vβ8.1 clonotype and $IGRP_{206-214}$-reactive cells were significantly attenuated in the
282 islets of T cell conditional OCA-B deficient mice (Fig. 2C-E, Fig. 3A-C), we crossed the *Ocab*
283 germline allele to the NY8.3 TCR transgenic line, which expresses a CD8-restricted TCR directed
284 towards $IGRP_{206-214}$ and manifests spontaneous T1D (Verdaguer et al., 1997). We passively monitored
285 *Ocab*$^{-/-}$ or control *Ocab*$^{+/+}$ NY8.3 mice for T1D development. Significant protection was observed
286 (Fig. 4G, HR=0.4472, p=0.0352), though the degree of protection was less than in OCA-B germline
287 knockout polyclonal models. Together with the decreased IGRP reactivity in OCA-B deficient PLNs,
288 this result indicates that OCA-B promotes T1D in peripheral auto-reactive $CD8^+$ T cells. Using
289 immunoblotting with OCA-B antibodies, we confirmed that OCA-B is expressed in primary splenic
290 C57BL/6 $CD8^+$ T cells. Unlike $CD4^+$ cells where OCA-B is undetectable in naïve cells but becomes
291 induced with prolonged activation (Fig. 4H, top panels), OCA-B^+ could be detected in naïve $CD8^+$
292 cells was rapidly augmented upon activation (Fig. 4H, lanes 1-2). Similar to $CD4^+$ cells, expression
293 was stably maintained when the stimulus was removed and cells were rested with IL-2 (lane 6).
294
295 **OCA-B deficiency promotes $CD4^+$ T cell anergy in vitro**
296 CD8-restricted TCR clones associated with T1D are depleted from the islets of OCA-B T cell
297 conditional mice. In contrast, CD4-restricted clones are increased but associated with an anergic
298 phenotype (Fig. 2E). Anergy is a peripheral tolerance mechanism in which T cells that encounter

299 antigen without co-stimulation become nonfunctional (Kalekar et al., 2016; Kearney et al., 1994;
300 Vanasek et al., 2001). Normal naïve primary $CD4^+$ T cells can be activated in culture by TCR and
301 costimulatory receptor activation, e.g. with anti-CD3ε/CD28 antibodies. Providing TCR signals
302 without CD28 antibodies generates anergic responses (Chai and Lechler, 1997). Interestingly, OCA-B
303 is induced to the same extent with or without co-stimulation (Fig. 5A). To determine if OCA-B loss
304 promotes anergic $CD4^+$ T cell responses, we stimulated naïve splenic $CD4^+$ T cells from germline
305 knockout *Ocab*$^{-/-}$ and control *Ocab*$^{+/+}$ animals ex vivo using plate-bound anti-CD3ε antibodies without
306 co-stimulation, and restimulated the cells with PMA/ionomycin. IL-2 responses were weak in
307 restimulated cells, as expected given the absence of initial costimulation. $CD4^+$ T cells lacking OCA-B
308 generated ~2.5-fold less IL-2 (Fig. 5B,C), indicating that OCA-B provides a barrier against anergic
309 responses.
310 In $CD4^+$ cells, ICOS (Inducible T-cell costimulator) promotes the induction of T cell anergy
311 (Dong et al., 2001; Dong and Nurieva, 2003; Tuettenberg et al., 2009) and is up-regulated by Oct1 loss
312 in naïve T cells subjected to stimulation under anergic conditions (Kim et al., 2019). Oct1 loss also
313 elevates expression of FR4 and CD73 (Kim et al., 2019) the co-expression of which is a marker for
314 anergy (Kalekar et al., 2016; Martinez et al., 2012). To determine whether OCA-B loss similarly
315 affects expression of these proteins, we stimulated naïve splenic $CD4^+$ T cells
316 ($CD8a^{neg}CD11b^{neg}CD45R^{neg}DX5^{neg}Ter\text{-}119^{neg}CD44^{lo}$) from 6 wk-old *Ocab*$^{fl/fl}$CD4-cre and littermate
317 control CD4-cre male NOD mice for 2 d ex vivo using anti-CD3ε antibodies ± costimulation. Cells
318 were then rested for an additional 2 d. Across all conditions, $CD4^+CD44^+FR4^{hi}CD73^{hi}$ anergic cells
319 were present at >2-fold higher frequency in the OCA-B deficient condition (Fig. 5D). The fraction of
320 $CD44^+$ cells that express ICOS was similarly elevated in cells lacking OCA-B, though only without
321 costimulation (Fig. 5E). Additionally, the expression of the activation marker CD25 was slightly
322 decreased (Fig. 5F). Cumulatively these results suggest that OCA-B loss in $CD4^+$ T cells institutes
323 higher immune thresholds by augmenting anergic responses.
324
325 **Generation of an OCA-B peptide inhibitor**
326 The normal T cell developmental and primary immune response phenotypes observed with OCA-B
327 genetic deletion suggested the possibility of a "therapeutic window" in which targeting OCA-B
328 pharmacologically would blunt autoimmunity while minimally affecting baseline immune function.
329 Based on available OCA-B structural information, we generated a membrane-permeable peptide
330 inhibitor of OCA-B's downstream effector functions. Oct1 interacts with Jmjd1a in a MEK/ERK-

331 dependent manner (Shakya et al., 2015; Shakya et al., 2011) and contains two potential ERK phospho-
332 acceptor serines. The structure of the Oct1 DNA binding domain complexed with consensus octamer
333 binding site DNA (Klemm et al., 1994) reveals that these Oct1 serines are located in the flexible,
334 solvent-exposed linker domain, which connects the two DNA binding sub-domains (Fig. 6A, red
335 dashed line). In contrast with Oct1, OCA-B constitutively interacts with Jmjd1a (Shakya et al., 2015).
336 The OCA-B N-terminus has been solved in complex with the Oct1 DNA binding domain and
337 consensus octamer DNA (Chasman et al., 1999). This region of OCA-B is critical for both Oct1
338 binding and transcription activity (Gstaiger et al., 1996). To identify potential Jmjd1a-interacting
339 OCA-B regions, we aligned the full-length Oct1 and OCA-B amino acid sequences to a cofactor
340 interaction surface of androgen receptor (AR), which also interacts with Jmjd1a (Yamane et al., 2006).
341 Human AR mutations that cause androgen insensitivity have been mapped to residues 698-721 (Thin et
342 al., 2002). Aligning this span to Oct1 identifies the linker domain as the top hit (Fig. 6B). The
343 alignment shows conservation of 3 out of 4 deleterious AR mutations (asterisks). The mutation site that
344 is not conserved is a potential ERK target serine in Oct1, and a phospho-mimetic glutamic acid residue
345 in AR (blue box). These findings suggest that the Oct1 linker domain constitutes a surface which when
346 phosphorylated interacts with Jmjd1a.
347 As with Oct1, alignment with OCA-B identifies a potential Jmjd1a interacting surface (Fig.
348 6B). Unlike Oct1, a glutamic acid residue (Glu30) aligns with AR. Furthermore, the OCA-B residues
349 aligning to AR lie on one side of an alpha-helix (Fig. 6A). Glu30 (red), Leu31 (yellow), Arg34 (blue)
350 and His38 (blue) may therefore constitute a Jmjd1a docking surface. These residues are conserved
351 between mouse and human (Fig. 6C). We mutated OCA-B L31 and R34 to alanine in a transient
352 expression plasmid, and transfected the double-point mutant or parent plasmid control into HCT116
353 cells, which do not express endogenous OCA-B. Control co-IP using Jmjd1a antibodies and lysates
354 from cells expressing wild-type OCA-B confirms the interaction (Fig. 6D, lane 5), while the mutant
355 OCA-B protein failed to interact (lane 8). The mutant was expressed equivalently to WT (lanes 2, 3).
356 These results show the importance of OCA-B residues 30-38 for cofactor interactions.
357 We synthesized three overlapping peptides corresponding to the OCA-B N-terminus (Fig. 6E,
358 peptides #1, #2 (hereafter called "JumOCA") and #3), as C-terminal fusions to the HIV Tat protein for
359 membrane permeability (Schwarze et al., 2000). We also conjugated HIV Tat to FITC to enable
360 peptide tracking. Incubating total splenic or pancreatic $CD3^+$ T cells in ex vivo culture with 45 μM Tat-
361 fused peptide for 15 min significantly concentrated the peptide within cells. Control OVA-fused
362 peptide lacking membrane-penetrating properties showed no effect (Fig. S5). We then treated splenic
363 $CD4^+$ T cells with the Tat-fused JumOCA peptides. Prior work has shown that 6 hr restimulation of

364 resting but previously activated OCA-B deficient $CD4^+$ T cells results in decreased expression of target
365 genes such as *Il2* (Shakya et al., 2015). Using this assay with 50 μM JumOCA peptide (every other day
366 with media changes during rest and restimulation) inhibited *Il2* mRNA expression relative to β-actin
367 by ~10-fold (Fig. 6F, compare Tat peptide to JumOCA). Although treated cells showed no obvious
368 changes in viability, morphology or expansion during the course of the assay (not shown), there was a
369 2-3-fold nonspecific diminution of activity associated with unfused Tat peptide (Fig. 6F, compare Tat
370 peptide with no peptide), which has been associated with toxicity (Caron et al., 2004; Krautwald et al.,
371 2004; Polo et al., 2004). Similar results were obtained with the larger peptide #3 but not with peptide
372 #1 (not shown). Peptide #1 is missing residues important for the Jmjd1a interaction based on
373 mutagenesis (Fig. 6B). For all further experiments, we used the JumOCA peptide.
374 We then synthesized a Tat-conjugated peptide using a scrambled JumOCA sequence. This
375 peptide has the same amino acid composition, mass and pI, but should not be able to efficiently
376 compete for Jmjd1a. We used the Tat-only, scrambled and JumOCA peptides with flow cytometry to
377 assess IL-2 production in restimulated $CD4^+$ T cells. JumOCA significantly inhibited IL-2 production
378 relative to the scrambled control, however there were significant toxicities associated with both the
379 scrambled and Tat-only peptides relative to vehicle (Fig. 6G). An example mouse from this experiment
380 is shown in Fig. 6H.
381 The above results are consistent with the JumOCA peptide operating via Jmjd1a competitive
382 inhibition. To test this directly, we used scrambled, double point mutant and wild-type (JumOCA)
383 peptides (lacking the Tat membrane penetrating domain) in a Jmjd1a co-IP assay. We subjected lysates
384 from mouse M12 B cells, which expresses endogenous OCA-B, to immunoprecipitation with Jmjd1a
385 antibodies, resulting in OCA-B co-IP (Fig. 6I, lane 3). Incubation of precipitated material with
386 scrambled or double point mutant peptides had no effect on OCA-B co-immunoprecipitation (lanes 4-
387 5), while the same concentration of JumOCA peptide efficiently blocked OCA-B recovery (lane 6).
388
389 **JumOCA protects NOD mice from newly-arisen T1D**
390 By the time symptoms arise in NOD mice, 90-95% of beta cells have been destroyed. Remaining beta
391 cells are rendered nonfunctional due to insulitis. Alleviating this inflammation provides a "honeymoon
392 period" during which glucose homeostasis can be restored. We treated 12-18 wk littermate female
393 NOD mice whose glucose levels were newly-risen above 225 mg/dL but still below 275 mg/dL with
394 three intravenous injections of 10 mg/kg JumOCA peptide or Tat-only peptide control. Injections were
395 spaced 12 hr apart. Immediately after the second injection and 4 hr after the final injection, blood

396 glucose was measured. Strikingly, JumOCA but not Tat-only or scrambled peptide reversed elevated
397 blood glucose (Fig. 7A). Islet T cell pro-inflammatory IFNγ and IL-17A cytokine production were
398 reduced by JumOCA peptide treatment compared to Tat-only controls (Fig. 7B,C). In contrast to the
399 pancreas, PLNs showed no change in T cell numbers or percentages (Fig. 7D) but similar decreases in
400 pro-inflammatory cytokine production (not shown).

401 Autoantigen-specific $CD8^+$ T cells in the PLNs of prediabetic, OCA-B deficient animals are
402 present but poorly activated by self-peptide (Fig. 3D,E). We treated animals with three injections of
403 JumOCA or scrambled peptide control, and stimulated PLN WBCs with IGRP self-peptides as in Fig.
404 3D. Significant reductions in IFN expression were observed in JumOCA-treated animals compared to
405 controls (Fig. 7E). Quantification from multiple mice is shown in Fig. 7F. These data show that
406 JumOCA peptide treatment decreases $CD8^+$ T cell autoreactivity within the PLNs, similar to genetic
407 OCA-B deletion. Cumulatively, these data provide evidence that targeting OCA-B is a valid strategy to
408 treat emerging T1D, and identify a first-generation inhibitor that is efficacious in vivo.

409 **Discussion**

410 Autoimmune therapies aim to inhibit autoreactivity while preserving normal immune function. Here
411 we show that genetic and pharmaceutical targeting of OCA-B blocks T1D in mouse models. Although
412 potentially autoreactive $CD8^+$ T cell specificities are still generated and appear in the PLNs of OCA-B
413 T cell deficient mice, they fail to become activated and do not accumulate in the pancreas. In contrast,
414 potentially autoreactive $CD4^+$ T cells are present but associated with anergic cell populations. OCA-B
415 is not expressed during thymic development or in naïve $CD4^+$ T cells, but is stably induced upon
416 activation. In contrast, OCA-B is expressed in naïve $CD8^+$ T cells and rapidy increased upon
417 activation.

418 In $CD4^+$ T cells, OCA-B associates with the POU-domain transcription factor Oct1 at ~150
419 immunomodulatory genes – among them *Il2*, *Ifng* and *Csf2* (*Gmcsf*). Unlike transcription factors such
420 as NF-AT, AP-1 and NF-kB that act as primary "on" switches, OCA-B removes inhibitory chromatin
421 modifications to establish permissive chromatin environments that allow for silent but previously
422 activated targets to be robustly expressed upon antigen re-encounter (Shakya et al., 2015; Shakya et al.,
423 2011). More specifically, OCA-B interacts with Jmjd1a, a histone lysine demethylase that removes
424 inhibitory histone H3 lysine 9 methyl marks. In vivo, OCA-B loss preserves T cell development and
425 pathogen response, but impairs the establishment of new central memory $CD4^+$ T cells. The few cells
426 that are formed respond poorly to antigen re-encounter (Shakya et al., 2015). Repeated antigen
427 encounters that drive high levels of proinflammatory cytokines are a key feature of autoimmunity. In
428 both mice and humans, memory or memory-like cells can underlie autoimmunity including T1D (Chee
429 et al., 2014; Kawakami et al., 2005; Yeo et al., 2018).

430 The NOD model of T1D is spontaneous but only partially penetrant, much like the human
431 disease (Parker et al., 2009). 60-80% of female NOD mice develop T1D in standard environments
432 (Makino et al., 1985). We find that prediabetic OCA-B T cell deficient NOD mice harbor normal T
433 cell numbers and TCR specificities in their PLNs, consistent with prior observations that OCA-B
434 deficient T cells are largely immunocompetent (Kim et al., 2019; Shakya et al., 2015). Nevertheless, T
435 cell conditional OCA-B knockouts are protected from spontaneous T1D. Whole-body NOD *Ocab*
436 knockouts are also protected from T1D. Prior work showed that OCA-B whole-body knockout protects
437 mice both from lupus-like disease mediated by loss of *Izkf3*/*Aiolos* (Sun et al., 2003), and in a
438 MOG/EAE model of multiple sclerosis (Ikegami et al., 2019). In contrast, a third study showed
439 exacerbation of systemic, antibody-driven autoimmunity in *Sanroque* mice (Chevrier et al., 2014). The
440 protective vs. exacerbating effects in whole body knockouts may be due to effects on class switching
441 and affinity maturation in germinal centers vs. effects on BCR repertoire (Casellas et al., 2002). A

442 whole body OCA-B knockout also reduces fat accumulation and insulin resistance in aged mice, likely
443 through ablation of B cell-mediated inflammation in white adipose tissue (Carter et al., 2018). T cell-
444 specific knockout of Oct1, a transcription factor with which OCA-B docks, blocks EAE but preserves
445 responses to infection with neurotropic viruses (Kim et al., 2019). Together these data show that in T
446 cells Oct1 and OCA-B promote autoimmunity including T1D, but that their role in B cells may be
447 more complex. OCA-B is typically expressed 50-100-fold higher in B cells compared to T cells. A
448 correctly calibrated dose of competitive inhibitor could therefore be used to selectively blunt T cell-
449 mediated autoimmunity.

450 scRNAseq experiments reveal decreased pancreatic neutrophil infiltration and an increased
451 percentages of T cells with naïve phenotypes in prediabetic OCA-B conditional knockouts. Gene
452 expression changes were identified consistent with antidiabetogenic effects of OCA-B T cell knockout.
453 For example, the remaining islet neutrophils in knockout mice show reductions in *Cxcl2* expression.
454 Cxcl2 is a potent neutrophil chemoattractant that promotes T1D in vivo (Citro et al., 2015; Diana and
455 Lehuen, 2014). Strikingly, OCA-B T cell deficient mice also lack T1D-associated TCR clones in their
456 activated/memory CD8 pool. Flow cytometry using class I tetramers show a significant reduction in
457 $CD8^+$ T cells specific for the $IGRP_{206-214}$ autoantigen. PLN $CD8^+$ T cells reactive to this and other
458 autoantigens show reduced reactivity to peptide stimulation ex vivo, suggesting that these autoreactive
459 $CD8^+$ cells are produced in the thymus but fail to become activated in the PLNs. In contrast, CD4
460 clonotypes associated with T1D are present in the pancreata, but associated with anergic gene
461 expression profiles. Consistently, OCA-B loss promotes $CD4^+$ T cell anergy in vitro. Loss of Oct1, the
462 transcription factor with which OCA-B docks, also augments anergic responses (Kim et al., 2019).

463 C57BL/6.RIP-mOVA and NOD.BDC2.5 transgenic mice are simplified monoclonal systems
464 that allow tracking of uniform T cell responses to antigens in vivo (Haskins, 2005). RIP-mOVA
465 expresses synthetic membranous chicken ovalbumin in thymic epithelial and pancreatic beta cells
466 (Kurts et al., 1996; Van Belle et al., 2009). Disease in can be induced in this model in 6-10 d by the
467 addition of OT-I T cells and infection with the OVA-expressing *Listeria*. OCA-B loss in host T cells
468 has no effect in this model. BDC2.5 autoreactive T cells migrate to the islets and cause insulitis
469 beginning at 3-4 weeks (Katz et al., 1993). Due in part to Tregs that have escaped allelic exclusion, in
470 many animals insulitis is limited and does not progress to T1D. However, transferring
471 $CD4^+CD62L^+V\beta^+$ or $CD4^+CD25^-$ T cells from BDC2.5 donor mice into NOD.SCID recipients also
472 results in rapid (7-10 d) disease onset (Berry and Waldner, 2013). Transplants from both control and
473 OCA-B null NOD/BDC2.5 mice results in disease with similar kinetics. Identical results were

474 generated by depleting $CD25^+$ Tregs, or by transplanting total $CD4^+$ T cells into immunodeficient
475 NCG recipient mice.
476 NOD.NY8.3 TCR transgenic mice carry a monoclonal CD8-restricted TCR directed towards
477 $IGRP_{206-214}$ and manifest spontaneous T1D (Verdaguer et al., 1997). Unlike transplantation models,
478 OCA-B T cell conditional NY8.3 mice show significant protection from spontaneous T1D.
479 Cumulatively, the results support a model in which OCA-B loss preserves T cell functionality while
480 desensitizing autoreactive T cells. This results in graded protection that drops off using models in
481 which protection is inseparable from immunodeficiency. These properties make OCA-B a promising
482 target for pharmaceutical inhibition.
483 Recent work indicates that the prevailing idea that transcription regulators and protein-protein
484 interactions are "undruggable" is erroneous (Antony-Debre et al., 2017; Green, 2016; Skwarczynska
485 and Ottmann, 2015; Zuber et al., 2011). Pre-clinical membrane-penetrating peptides have also been
486 developed that successfully target transcription factors such as BCL6 (Polo et al., 2004). We applied
487 rational-design principles to generate a membrane-permeable competitive peptide inhibitor of the
488 interaction between OCA-B and a downstream effector, Jmjd1a/Kdm3a. The sequence of the inhibitor,
489 termed JumOCA, does not coincide with other sequences in the human or mouse proteome and is not
490 predicted to be strongly immunogenic. JumOCA administration blunts newly-arisen T1D in NOD mice
491 and significantly reduces islet T cell cytokine production. Total T cell numbers were unaffected,
492 however PLN $CD8^+$ T cell autoreactivity to IGRP peptides was blunted, similar to T cell knockouts.
493 OCA-B levels in B cells are at least 50-fold higher than in T cells (Heng et al., 2008; Zwilling et al.,
494 1997), making it likely that the observed effects are due to inhibition in T cells. Consistently, three
495 JumOCA injections has no effect of splenic germinal center architecture (not shown), which is known
496 to depend OCA-B expression in B cells (Qin et al., 1998). More than three peptide injections results in
497 toxicity (not shown), complicating experiments testing T1D prevention and durable response. Tat-
498 conjugated peptides are known to be associated with toxicity (Caron et al., 2004; Krautwald et al.,
499 2004; Polo et al., 2004). While these peptides are unlikely to be used in a clinical setting, they offer
500 proof-of-principle for OCA-B as a therapeutic target, and can be used as tools for the further
501 development of therapeutics with the caveat that targeting this pathway would likely inhibit the
502 generation of new memory $CD4^+$ T cells.

503 **Author contributions**

504 DT conceived the study and designed experiments, supervised the study, and provided administrative
505 and material support. HK, AS, AI and JLJ acquired and interpreted the data. JP performed analysis of
506 scRNAseq and TCR clonotype data. CG and NPL helped generate critical reagents. BDE, DH-CC, XH
507 and PJ provided material and intellectual support. All authors were involved in writing, reviewing and
508 revising the manuscript.

509

510 **Acknowledgements**

511 We thank P. Santamaria, M. Williams, M. Bettini and F. Gounari for critical reading of the manuscript.
512 We thank A. Chervonsky (U. Chicago) for the gift of NOD.CD4-cre mice. We thank J. Marvin and the
513 University of Utah Health Sciences Center Flow Cytometry Core facility for assistance with flow
514 cytometry, and D. Lum and the Preclinical Resource Core for immunodeficient mice. We thank M.
515 Hanson and the University of Utah Health Sciences DNA/peptide synthesis core. This work was
516 supported by grants to DT from the Praespero Foundation, Juvenille Diabetes Research Foundation (1-
517 INO-2018-647-A-N) and National Institutes of Health (R01-AI100873).

518

519

520 Disclosures: The authors declare that they have no conflicts of interest regarding this work.

521 **Materials and methods**

522 **Mice**

523 All animal experiments were approved by the University of Utah Institutional Animal Care and Use
524 Committee (IACUC approval 17-05008). NOD/ShiLtJ, NOD.Scid (NOD.Emv302/2.CB17-Prkdcscid),
525 BDC-2.5 TCR transgenic, NY8.3 TCR transgenic and all breeder mice were maintained in a specific
526 pathogen-free research colony. NCG (NOD-Prkdc^{em26Cd52}Il2rg^{em26Cd22}/NjuCrl) mice were purchased
527 from Charles River Laboratories. NOD.CD4-cre mice were a gift from Alexander Chervonsky
528 (University of Chicago). *Pou2af1*$^{tm1a(KOMP)Wtsi}$ mice were provided by the knockout mouse project
529 (KOMP) repository (University of California, Davis). Mice were derived from embryonic stem cell
530 clone EPD0761_3_B03, generated by the Wellcome Trust Sanger Institute. These cells were derived
531 from C57BL/6N mice, but subsequent mouse crosses were to C57BL/6J (>20 generations) for the RIP-
532 mOVA model and NOD (4 congenic backcrosses plus an additional backcross to NOD.CD4-cre). The
533 embryonic stem cells contain a CSD-targeted allele (Testa et al., 2004). The presence of WT (582 bp)
534 and Post-FLP (700 bp) alleles was determined by PCR using CSD-Pou2af1-F and CSD-Pou2af1-ttR
535 primers. The presence of the null (801 bp) allele was determined using CSD-Pou2af1-F and CSD-
536 Pou2af1-R primers. The presence of the floxed (359 bp) allele was determined using CSD-Lox-F and
537 CSD-Pou2af1-R primers. Primer sequences were as follows: CSD-Pou2af1-F,
538 5'TACAGAGAGACTAGACACGGTCTGC; CSD-Pou2af1-R,
539 5'GATGAGGACTCTGGGTTCAGAGAGG; CSD-loxF, 5'GAGATGGCGCAACGCAATTAATG;
540 CSD-Pou2af1-ttR, 5'AGAAGGCCTCGTTACACTCCTATGC.

541

542 **Backcrossing *Ocab* germline null and conditional mice to the NOD background**

543 To generate *Ocab*$^{-/-}$ and *Ocab* conditional mice on the NOD background, the previously described
544 C57BL/6 *Ocab* germline null allele (Kim et al., 1996) and the newly-generated *Ocab* conditional allele
545 were backcrossed to NOD ShiLt/J mice using congenic markers based on Mouse Genome Informatics
546 (http://www.informatics.jax.org) (Table S1).

547

548 **Diabetes development and assessment**

549 Diabetes was monitored using blood glucose test strips (Contour, Bayer). Mice with blood glucose
550 levels >250 mg/dL were considered diabetic.

551

552 **Leukocyte isolation and flow cytometry**

553 PLNs were disaggregated and passed through a nylon strainer. Pancreatic leukocytes were isolated as
554 described previously (Sitrin et al., 2013). Briefly, pancreata were chopped and digested using
555 collagenase IV (1 mg/mL, Gibco) in DMEM containing 1% fetal bovine serum (FBS, Rocky Mountain
556 Biologicals) and 10 units of DNase I for 15 min at 37°C. The digested tissues were passed through a 70
557 μm strainer. Red blood cells were lysed by ACK (Ammonium-Chloride-Potassium) lysis buffer (150
558 mM NH_4Cl, 10 mM $KHCO_3$, 0.1 mM Na_2EDTA). For intracellular cytokine staining, cell suspensions
559 in RPMI medium supplemented with 10% FBS were re-stimulated for 4 hr with phorbol 12-myristate
560 13-acetate (PMA, Sigma, 50 ng/mL) and ionomycin (Sigma, 1 μg/mL) in the presence of brefeldin A
561 (GolgiPlug, BD Bioscience, 1 μl/ml), and fixed by cell fixation/permeabilization solution (BD
562 Cytofix/Cytoperm) according to the manufacturer's protocol. Antibodies used for flow cytometry were
563 as follows: FITC-conjugated anti-mouse CD4, PE-conjugated anti-mouse CD45, PE-conjugated anti-
564 mouse FR4 (BioLegend), PerCP-conjugated anti-mouse CD8a, APC-conjugated anti-mouse IFNγ, PE-
565 conjugated anti-mouse IL-17, PerCP-conjugated anti-mouse CD11b, APC-conjugated anti-mouse
566 F4/80, PE-conjugated anti-mouse Gr-1, PE-conjugated anti-mouse ICOS (eBioscience), PerCP-
567 conjugated anti-mouse FoxP3, V450-conjugated anti-mouse CD73 (BD Bioscience) and FITC-
568 conjugated anti-mouse Vβ8.1/8.2 (Invitrogen). A FACS Canto II (BD Biosciences) was utilized for
569 flow cytometry, and FlowJo software was used for analyses.
570
571 **T cell adoptive transfer**
572 6–8 wk old NOD.Scid recipient mice were injected retro-orbitally with 2×10^5 of splenic $CD4^+CD25^-$ T
573 cells from prediabetic *Ocab*$^{-/-}$ or *Ocab*$^{+/+}$ NOD.BDC2.5 donors (6–8 wk old, sex-matched). T cells
574 were purified using a $CD4^+CD25^+$ T cell isolation kit (Miltenyi). For $CD4^+CD25^+$ T cells, 1.5×10^6
575 purified splenic $CD4^+$ T cells from prediabetic, BDC2.5 transgenic NOD.*Ocab*$^{-/-}$ or NOD.*Ocab*$^{+/+}$
576 mice were transferred to sex-matched 6-8 wk old NCG recipients (University of Utah Preclinical
577 Resource Core) as previously described (Presa et al., 2015). For total splenic transfer experiments,
578 5×10^6 splenocytes from prediabetic NOD.*Ocab*$^{fl/fl}$ or NOD.*Ocab*$^{fl/fl}$CD4-cre mice were transferred into
579 sex-matched 6-8 wk NOD.Scid recipients mice as described previously (Presa et al., 2015).
580
581 **In vitro T cell culture**
582 For anergic cell induction, spleens were harvested from NOD.*Ocab*$^{fl/fl}$CD4-cre or control NOD.*Ocab*$^{fl/fl}$
583 animals. Single-cell suspensions were generated by grinding and passage through 70 μm strainers.
584 Cells were isolated using a mouse $CD4^+$ T cell isolation kit (Miltenyi Biotec), and stimulated with

585 5 μg/ml plate-bound anti-CD3ε (BD Bioscience) ± 2 μg/ml anti-CD28 antibody (eBioscience) as
586 described previously (Kim et al., 2019). For OCA-B inhibitor peptide treatments, cells were isolated
587 from WT C57BL/6 spleens using a mouse naïve $CD4^+$ T cell isolation kit (Miltenyi Biotec) and
588 cultured as described previously (Shakya et al., 2011). Indicated concentrations of peptides were
589 incubated with cells, with media changes every 2 days after primary stimulation. Activation of
590 C57BL/6 $CD4^+$ cells and subsequent profiling of anergic responses was performed identically to (Kim
591 et al., 2019). For peptide restimulation, total WBCs from PNLs were incubated with 10 μg/mL
592 specific peptide for 4 hr in the presence of brefeldin A. The peptides used were as follows: $GAD65_{206-}$
593 $_{214}$, TYEIAPVFV; $GAD65_{546-554}$, SYQPLGDKV; $IGRP_{21-29}$, TYYGFLNFM; $IGRP_{206-214}$,
594 VYLKTNVFL; $IGRP_{225-233}$, LRLFGIDLL; $IGRP_{241-249}$, KWCANPDWI; $IGRP_{324-332}$, SFCKSASIP.
595 Cells were then fixed and stained for flow cytometry.
596
597 **Single-cell RNA sequencing (GEO Series record GSE145228)**
598 $CD3^+$ T cells were isolated from 8 wk NOD.*Ocab*$^{fl/fl}$ or NOD.*Ocab*$^{fl/fl}$CD4-cre females using a pan T
599 cell isolation kit (Miltenyi). $CD45^+$ pancreatic leukocytes were isolated from 12 wk NOD.*Ocab*$^{fl/fl}$ or
600 NOD.*Ocab*$^{fl/fl}$CD4-cre females were isolated by flow cytometry using a FACS Aria (Becton-
601 Dickinson). For each condition, cells were isolated from three mice and combined. Cells were
602 processed using the 10X Genomics Chromium platform according the manufacturer's instructions.
603 Paired-end high-throughput sequencing (125 cycles) was performed via an Illumina NovaSeq
604 instrument. Sequencing reads were processed by using 10X Genomics CellRanger pipeline and further
605 analyzed using the Seurat R package. Analysis of cells used a standard filtering protocol removing
606 cells with unique feature counts of >4,000 or <500, as well as cells with >5% mitochondrial counts
607 (indicative of dead cells). No more than 15% of total cells were removed by this process. Cells were
608 subjected to unsupervised hierarchical clustering followed by uniform manifold approximation and
609 projection (UMAP) to visualize clusters with similar gene expression and their relative positions.
610
611 **Tetramer staining**
612 H-$2K^d$ mouse $IGRP_{206-214}$ tetramers (Mouse NRP-V7 mimotope KYNKANVFL) conjugated to APC
613 or PE were synthesized by the NIH tetramer core facility and were a gift of Dr. Maria Bettini
614 (University of Utah).
615
616 **OCA-B mutagenesis and Co-IP**

617 For generation of the OCA-B double point mutant, a plasmid transiently expressing human OCA-B,
618 pCATCH-Bob.1 (Gstaiger et al., 1995), was sequentially mutagenized using QuickChange
619 (ThermoFisher). Correct mutagenesis was confirmed by resequencing. HCT116 lysate preparation, co-
620 immunoprecipitation of OCA-B and endogenous Jmjd1a, and immunoblot detection was performed
621 using the same conditions as described (Shakya et al., 2015). For co-IP using M12 cells, lysis buffer
622 consisted of 50 mM Tris-Cl, pH 7.4, 150mM NaCl, 0.5%NP-40, 1 mM EDTA, 1 mM EGTA, plus
623 protease/phosphatase inhibitors (PhosSTOP, Roche). Lysates were incubated with 2.5 µg Jmjd1A
624 antibody (Bethyl) and protein-G Dynabeads (ThermoFisher) in lysis buffer containing 20% glycerol
625 overnight at 4°C. After overnight incubation, the indicated concentrations of peptide or PBS vehicle
626 was added and incubated for a further 3 hr at 4°C prior to bead precipitation and washing 3× in lysis
627 buffer plus 20% glycerol. Co-precipitated OCA-B was analyzed by SDS-PAGE and immunoblot.
628
629 **OCA-B inhibitor peptide synthesis**
630 Unique chemically synthesized peptide sequences were as follows: Peptide#1, ARPYQGVRVKEPVK;
631 Peptide#2/JumOCA, VKELLRRKRGH; Peptide#3, ARPYQGVRVKEPVKELLRRKRGH; Scrambled
632 peptide, VLREKGKRHLR. Peptides were synthesized with and without a covalent C-terminal linker
633 and Tat membrane-penetrating peptide (GSG-GRKKRRQRRRGY). Fmoc protected amino acids were
634 obtained from Protein Technologies Inc. 1-[Bis(dimethylamino)methylene]-1H-1,2,3-triazolo[4,5-
635 b]pyridinium 3-oxid hexafluorophosphate (HATU) was purchased from Chemimpex Inc. H-Rink-
636 Amide-ChemMatrix (RAM) was purchased from Biotage. N,N-diisopropylethylamine (DIEA),
637 dichloromethane (DCM), triisopropylsilane (TIS) were purchased from Sigma. Dimethylformamide
638 (DMF), trifluoroacetic acid (TFA), acetonitrile, and ethyl ether were purchased from Fisher Scientific.
639 Peptides were synthesized using automated Fmoc SPPS chemistry (Syro I). Briefly, 220 mg of RAM
640 resin (loading=0.45 mmol/g) was swelled in DCM for 15 min and followed by adding a solution of
641 specific Fmoc protected amino acid (AA = 0.1 mmol, DIEA = 0.2 mmol in DCM = 4 mL) and
642 incubated at room temperature for 1.5 h. The resin was washed with DMF and DCM and incubated
643 with 5 mL of DCM containing 16% v/v MeOH and 8% v/v DIEA for 5 min. This action was repeated
644 5 times before thoroughly washing with DCM and DMF. Coupling reactions were performed using
645 HATU (5 eq.), DIPEA (10 eq.) and amino acid (5 eq.) in DMF with 15 min heating to 70°C (50°C for
646 Cys). Deprotection was performed using 20% (v/v) piperidine in DMF, 5 min at room temperature for
647 2 rounds. Peptides were cleaved from the resin by treatment with a cocktail buffer (3 mL/0.1 mmol,
648 TFA:H2O:TIS:EDT = 95:2:2:1) for 2.5 h. Peptide-TFA solution was then filtered and precipitated in

649 cold ether, centrifuged, washed with ether twice and vacuum-dried. The crude product was then
650 purified by RP HPLC. Peptide characterization was performed by LC/MS on an Xbridge C18 5 µm (50
651 x 2.1 mm) column at 0.4 mL/min with a water/acetonitrile gradient in 0.1% formic acid on an Agilent
652 6120 Quadrupole LC/MS system. Fractions collected from HPLC runs were also analyzed by LC/MS.
653 The purified fractions containing the targeted product were collected and lyophilized using a Labconco
654 Freeze Dryer. All samples were analyzed by the following conditions: Preparative reverse phase HPLC
655 of crude peptides was performed on a Jupiter 5 µ C18 300 Å (250×10 mm) column at 3 mL/min with a
656 water/acetonitrile gradient in 0.1% TFA on an Agilent 1260 HPLC system. Purity, isomer co-injection
657 and stability checks were performed on HPLC on Phenomenex Gemini C18 3 µm (110 Å 150×3 mm)
658 column.
659
660 **OCA-B inhibitor peptide treatment**
661 Anesthetized prediabetic WT NOD females with glucose levels newly-risen to between 225 to 275
662 mg/dL were treated with 10 mg/kg inhibitor or control peptides by intravenous (retro-orbital) injection,
663 3 times every 12 hr. Blood glucose levels were measured after the 2nd and 3rd injection. 4 hr after the
664 last injection, pancreata and PLNs were collected and cell populations were analyzed by flow
665 cytometry.
666
667 **Histology**
668 Formalin-fixed pancreatic tissues were embedded in paraffin. H&E-stained sections were scored for
669 islet inflammation based on published precedents (Zhang et al., 2007): 0, sparse surrounding sentinel
670 leukocytes, no insulitis; 1, peri-islet leukocytes; 2, some islet leukocytes, <50% of islet area; 3, islet
671 insulitis with >50% of islet area occupied by leukocytes; 4, islets destroyed with fibrotic remnants.
672
673 **Statistical analyses**
674 All error bars denote ±SEM. Two-tailed student T-tests were used to ascribe statistical significance.
675 For all figures, *=$p \leq 0.05$; **=$p \leq 0.01$; ***=$p \leq 0.001$; ****=$p \leq 0.0001$.
676
677 **Online supplemental material**
678 Fig. S1 outlines the construction and validation of the *Ocab* (*Pou2af1*) conditional mouse allele. Fig.
679 S2 shows results from scRNAseq using PLNs from 8 week-old prediabetic female NOD.*Ocab*$^{fl/fl}$CD4-
680 cre or littermate control NOD.*Ocab*$^{fl/fl}$ mice. Fig. S3 shows TCR representation across all populations
681 based on scRNAseq from islet CD45^{+} cells. Fig. S4 shows results from BDC2.5 T cell transfer

682 experiment using OCA-B deficient and sufficient NOD mice, and results from RIP-mOVA T cell
683 transfer experiments using C57BL/6 mice. Fig. S5 shows the concentration of Tat-conjugated peptides
684 in cultured primary $CD3^+$ T cells.

685 **Figure legends**

686 Figure 1. **Loss of OCA-B protects NOD mice from T1D. (A)** Kaplan-Meier plot of diabetes-free
687 survival in littermate female NOD.*Ocab*$^{fl/fl}$CD4-cre (n=12) and NOD.*Ocab*$^{fl/fl}$ (n=14) mice. HR=hazard
688 ratio. **(B)** Average blood glucose levels from mice shown in panel A. Student T-test *p*-values: day 23,
689 0.0458; day 24, 0.0403; day 25, 0.494. **(C)** Percent diabetes-free survival in germline knockout
690 NOD.*Ocab*$^{-/-}$ (n=16) and control NOD.*Ocab*$^{+/+}$ (n=17) mice was plotted. **(D)** Pancreatic islet
691 leukocytes were isolated from 8 wk- or 24 wk-old littermate female NOD.*Ocab*$^{fl/fl}$CD4-cre (8 wk; n=3,
692 24 wk; n=5) or NOD.*Ocab*$^{fl/fl}$ (8 wk; n=3, 24 wk; n=4) mice and analyzed by flow cytometry. Mean
693 CD45$^+$CD11b$^+$F4/80$^+$ cell frequencies are depicted. Student T-test *p*-value=0.0397. **(E)** Frequencies of
694 CD45$^+$CD11b$^+$F4/80$^+$ cells from representative animals in D are shown. Plots were gated on CD45. **(F)**
695 Mean percentages of total pancreatic-infiltrating CD8$^+$ T cell in 9 experimental NOD.*Ocab*$^{fl/fl}$CD4-cre
696 or 11 littermate control NOD.*Ocab*$^{fl/fl}$ 12 wk-old mice are plotted. Cells were gated on CD45. **(G)** IFNγ
697 expressing CD8$^+$ T cell percentages in 16 wk old-NOD.*Ocab*$^{fl/fl}$CD4-cre (n=3) and littermate control
698 islets (n=5) are shown. Student T-test *p*-value=0.0477.

699

700 Figure 2. **T cell conditional OCA-B loss reduces the numbers of activated, autoreactive**
701 **pancreatic islet T cells. (A)** scRNAseq using total islet CD45$^+$ cells from prediabetic
702 NOD.*Ocab*$^{fl/fl}$CD4-cre or littermate control NOD.*Ocab*$^{fl/fl}$ mice (n=4 for each group). Cell populations
703 were plotted using UMAP (Seurat R package) and percentages in each cluster are shown for each
704 genotype. Clusters were identified using the Seurat R package function FindMarkers. **(B)** 4 clusters
705 from A were analyzed for differential gene expression. Identified genes are shown as a scatter plot.
706 Significantly differentially expressed genes (adjusted *p*-value <0.05) are shown in red. For *Cxcl2* in
707 neutrophils, $p=3.75\times10^{-6}$, adjusted *p*=0.055. **(C)** UMAP plots similar to A, except cells expressing
708 TCR clonotype 13-3 are shown. The non-naïve (activated+memory) CD8$^+$ cell population identified in
709 A is shown in red. **(D)** Percent contribution of the top 6 identified TCR clonotypes to total
710 activated+memory CD8$^+$ cells is shown. V genes comprising the clonotypes are shown below. **(E)**
711 Cells positive for clonotypes 1-5 are shown for two clusters, non-naïve (activated+memory) CD8$^+$ T
712 cells and CTLA4$^+$FR4$^+$ anergic cells (consisting of mostly CD4$^+$ cells). For each cluster, positive cells
713 are shown in dark blue. An overlay of control and OCA-B deficient cell populations is shown. Each
714 clonotype is only observed in a single genotype (panel D), allowing all cells to be mapped back
715 entirely to OCA-B deficient (clonotypes 1 and 4) or control (clonotypes 2, 3 and 5).

716

717 Figure 3. **Autoantigen-specific CD8+ cells become nonreactive and fail to infiltrate islets in the**
718 **OCA-B deficient condition. (A)** Pancreatic leukocytes were isolated from prediabetic 12 wk
719 littermate female NOD.*Ocab*$^{fl/fl}$CD4-cre (n=9) or NOD.*Ocab*$^{fl/fl}$ (n=10) mice and analyzed by flow
720 cytometry. Representative plots (left) and total CD8$^+$Vβ8.1$^+$ T cell numbers (right) are shown. Student
721 T-test *p*-value=0.030. **(B)** PLN leukocytes were isolated from same mice (NOD.*Ocab*$^{fl/fl}$CD4-cre, n=7
722 or NOD.*Ocab*$^{fl/fl}$, n=5) in A. Representative plots (left) and total CD8$^+$Vβ8.1$^+$ T cell frequencies (right)
723 are shown. Student T-test *p*-value=0.030. **(C)** Representative plots (left) and total cell numbers (right)
724 of CD8$^+$Vβ8.1$^+$ H-2K^d IGRP$_{206-214}$ tetramer-positive islet T cells are depicted from NOD.*Ocab*$^{fl/fl}$CD4-
725 cre (n=9) or NOD.*Ocab*$^{fl/fl}$ (n=10). Student T-test *p*-value=0.040. **(D)** Total PLN WBCs were isolated
726 from prediabetic 12 wk-old littermate NOD.*Ocab*$^{-/-}$ or NOD.*Ocab*$^{+/+}$ mice and re-stimulated with
727 IGRP peptides (IGRP$_{206-214}$ or IGRP$_{225-233}$). Cells were analyzed for IFNγ expression by flow
728 cytometry. **(E)** Mean percentages of cells expressing IFNγ from 9 experiments (3 replicates from 3
729 *Ocab*$^{+/+}$ and 3 *Ocab*$^{-/-}$ mice) for the peptides in D, as well as two GAD65 peptides (206-214 and 546-
730 554) and three additional IGRP peptides (21-29, 241-249 and 324-332). Significant student T-test *p*-
731 values were: GAD65$_{546-554}$, 0.046; IGRP$_{206-214}$, 0.005; IGRP$_{225-233}$, 0.030; IGRP$_{241-249}$, 0.004; IGRP$_{324-}$
732 $_{332}$, 0.012.
733
734 Figure 4. **OCA-B loss protects NOD mice from T1D in spontaneous and polyclonal splenocyte**
735 **transfer models but not monoclonal transfer models. (A)** 2×10^5 purified CD4$^+$CD25$^-$ splenic T cells
736 from NOD.BDC2.5.*Ocab*$^{-/-}$ or control NOD.BDC2.5.*Ocab*$^{+/+}$ donors were injected retro-orbitally into
737 NOD.Scid (n=6 for each group) mice. Diabetes-free survival is shown. **(B)** 1.5×10^6 purified splenic
738 total CD4$^+$ T cells from NOD.BDC2.5.*Ocab*$^{-/-}$ or control donors were transferred into NCG mice (n=5
739 for each group). Mice were monitored for diabetes development. **(C)** Total NOD splenocytes (5×10^6)
740 from prediabetic 6- to 8-wk-old NOD.*Ocab*$^{fl/fl}$CD4-cre or control NOD.*Ocab*$^{fl/fl}$ donors were
741 adoptively transferred into sex-matched NOD.Scid (n=7 for each group) recipients. T1D-free survival
742 is shown. **(D)** 13 wk post-transfer, the proportion of IFNγ-expressing islet CD8$^+$ T cells was assessed
743 by flow cytometry from mice in C. Student T-test *p*-value=0.0136. **(E)** Pancreata from the same mice
744 as in C were fixed, sectioned and H&E stained. Pathological scores are shown based on 6-7 islets/slide,
745 3 slides/mouse and 3 mice/group (>60 islets/group). Student T-test *p*-value=1.04×10^{-5}. **(F)** Example
746 pancreatic images from endpoint animals. Yellow arrows indicate islet positions. Images were
747 collected at 10× magnification. **(G)** The *Ocab* null allele was crossed to NY8.3 TCR transgenic mice.
748 Spontaneous T1D was measured in female *Ocab*$^{-/-}$ (n=20) or control *Ocab*$^{+/+}$ (n=12) littermates. **(H)**

749 Naïve $CD4^+$ or $CD8^+$ T cells ($CD8a^{neg}$ or $CD4^{neg}$,$CD11b^{neg}$,$CD45R^{neg}$,$DX5^{neg}$,Ter-119^{neg},$CD44^{lo}$) were
750 isolated from C57BL/6 spleens and stimulated for up to 2 d in vitro using anti-CD3ε and CD28
751 antibodies. Cells were then washed and replated in the presence of exogenous IL-2. After 8 d rest in
752 culture, cells were restimulated for 6 hr. Lysates were prepared from each step and subjected to OCA-
753 B immunoblotting to assess changes in expression. Oct1 and β-actin are shown as controls.
754
755 Figure 5. **OCA-B loss in $CD4^+$ T cells increases anergy in vitro. (A)** Naïve $CD4^+$ C57BL/6 T cells
756 were stimulated in vitro for 24 hr with anti-CD3ε antibodies ± co-stimulation with CD28 antibodies.
757 Lysates were prepared and subjected to immunoblotting using OCA-B antibodies. β-actin is shown as
758 a loading control. **(B)** Naïve OCA-B deficient and control $CD4^+$ T cells were stimulated in vitro with
759 anti-CD3ε antibodies. 48 hr later, the cells were re-stimulated with PMA and ionomycin for 6 hr in the
760 presence of brefeldin A, stained for intracellular IL-2 and analyzed by flow cytometry. Cells were
761 gated on CD4 and CD44. **(C)** Quantitation using independently purified cells from the spleens of 4
762 mice treated similar to B. Student T-test *p*-value=0.0019. **(D)** Naïve OCA-B deficient and littermate
763 control splenic $CD4^+$ T cells from 6 wk-old NOD mice were stimulated for 2 d in vitro with indicated
764 antibodies, replated and rested in the absence of antibody for 2 d, and analyzed by flow cytometry.
765 Mean $FR4^{hi}$ $CD73^{hi}CD4^+CD44^+$ cell frequencies are shown using independently purified cells from the
766 spleens of 2 mice, with 4 independent culture replicates performed for each mouse (n=8). Student T-
767 test *p*-values: CD3ε only, 0.0002; CD3ε/CD28, 1.04×10^{-5}; control CD3ε vs. CD3ε/CD28, 0.0053;
768 OCA-B deficient CD3ε vs. CD3ε/CD28, 0.0068. **(E)** Similar to D, except frequencies of
769 $CD4^+CD44^+ICOS^+$ cells are plotted. CD3ε only student T-test *p*-value=0.0026. **(F)** Similar to D,
770 except average percentage of $CD4^+CD44^+CD25^+$ cells are plotted. CD3ε only student T-test *p*-
771 value=1.80×10^{-5}.
772
773 Figure 6. **Design and validation of OCA-B peptide inhibitors. (A)** OCA-B N-terminus (residues 16
774 and 38)/Oct1 DNA binding domain/octamer binding DNA co-crystal structure (PDB ID 1CQT)
775 (Green, 2016). Gray: DNA. Green: Oct1 DNA binding domain. Cyan: OCA-B. Red dashed line shows
776 position of the Oct1 linker domain. **(B)** Top alignment of the human androgen receptor (AR) isoform
777 transcript variant 1 (Sequence ID: ADD26780.1) co-activator interaction domain (residues 698-721)
778 with full-length human Oct1 and OCA-B. The aligned regions are from the Oct1 linker domain and
779 OCA-B N-terminus. Green serines: putative ERK phospho-acceptor sites. Yellow: similar or identical
780 amino acids. Asterisks: known human point mutations that block coactivator binding and cause

781 androgen insensitivity syndrome in humans. Pairwise alignments were performed using the FASTA
782 algorithm (https://embnet.vital-it.ch/software/LALIGN_form.html) and trimmed for 3-way overlap.
783 **(C)** Alignment of human and mouse primary OCA-B peptide sequences. **(D)** Co-IP of Jmjd1a with
784 L31A/R34A double point-mutant OCA-B and wild-type control. HCT116 cells transfected with WT or
785 mutant OCA-B constructs were used. Protein expression was checked 48 hrs after transfection by
786 Western blotting. 50 μg input protein was loaded in lanes 1-3. **(E)** Indicated peptide sequences were
787 synthesized as C-terminal Tat fusions for membrane permeability. Arrows indicate position of mutant
788 in B and D. **(F)** *Il2* mRNA expression in primary naïve $CD4^+$ T cells treated with 50 μM JumOCA
789 peptide was measured relative to β-actin internal standard by RT-qPCR. Cells were stimulated with
790 CD3ε/CD28 antibodies for 2 d, rested for a further 8 d in the presence of exogenous recombinant IL-2,
791 and restimulated for 6 hr. Peptide was included during resting and restimulation only, and replaced
792 every other day with media changes. Three independent biological replicates were used for each
793 condition. Tat vs. JumOCA restim student T-test *p*-value=0.0007. Tat vs. vehicle student T-test *p*-
794 value=0.0022. **(G)** IL-2 cytokine expression in primary naïve $CD4^+$ T cells cultured with 50μM
795 peptide at initial treatment, and with 25μM peptide from the secondary treatment was measured by
796 flow cytometry. Cells were treated similarly to F except collection, brefeldin A treatment and
797 processing for flow cytometry occurred 24 hr post-restimulation. Three independent biological
798 replicates were used for each condition. Vehicle vs. JumOCA student T-test *p*-value=9.62×10^{-7}.
799 Scrambled peptide vs. JumOCA student T-test *p*-value=0.0006. **(H)** $CD4^+CD44^+IL2^+$ T cell
800 frequencies from representative samples in G. Plots were gated on CD4 and CD44. **(I)** Peptide effects
801 on the interaction between OCA-B and Jmjd1a was measured by co-immunoprecipitation. M12 B cells
802 were used. After incubation with protein-G beads, 0.2 μg/μL control scrambled (Scram), double point
803 mutant (DM) peptide or JumOCA peptide were added for a further 3 hr prior to precipitation and
804 washing. 1% input (lane 1) is shown as a control.
805
806 Figure 7. **OCA-B inhibitor peptide reduces blood glucose and inflammatory cytokine levels in the**
807 **pancreas in NOD mice with newly-arisen diabetes. (A)** 3 doses of 10 mg/kg JumOCA (n=4), Tat
808 only (n=6) or scrambled peptide (n=3) were injected retro-orbitally every 12 hr into 12-18 wk-old
809 NOD female littermate mice whose glucose levels were newly-risen above 225 mg/dL but still below
810 275 mg/dL. Glucose levels are shown immediately before the first injection, after the second injection
811 and 4 hr after the final injection. Data were collected on a rolling basis as mice became spontaneously
812 diabetic. JumOCA vs. Tat peptide student T-test *p*-value=0.0004. JumOCA vs. scrambled peptide

813 student T-test *p*-value=0.0064. **(B)** 12 hr after the last injection of peptides in A, PLN $CD4^+$ and $CD8^+$
814 T cell percentages were analyzed by flow cytometry. Mean of islet IL-17 expressing T cells were
815 analyzed by flow cytometry and plotted. Results are from 3 independent mice in the case of Tat and 4
816 independent mice in the case of JumOCA. $CD4^+IL\text{-}17^+$ student T-test *p*-value=0.002. **(C)** Similar
817 analysis as B except for IFNγ. $CD4^+$ student T-test *p*-value=0.0062. $CD8^+$ student T-test *p*-
818 value=0.0002. **(D)** Percentages of PLN $CD4^+$ and $CD8^+$ T cells from mice in A. **(E)** NOD mice were
819 treated with 3 intravenous peptide injections as before, except that 12-wk pre-diabetic mice were used
820 and scrambled peptide was additionally included as a control. 4 hr after the final injection, PLN WBCs
821 were stimulated with IGRP peptides and brefeldin A for 4 hr, stained for IFNγ and analyzed by flow
822 cytometry as in Figure 3D. Representative animals are shown. **(F)** Mean percentages of cells
823 expressing IFNγ from 6 experiments. $IGRP_{206\text{-}214}$ student T-test *p*-value=0.0244. $IGRP_{225\text{-}233}$ student T-
824 test *p*-value=0.0201.

825 **Supplemental information**
826
827 Figure S1. ***Ocab* (*Pou2af1*) conditional allele. (A)** Targeting event. Crossing with FLP^{Rosa26} results in
828 conditional (*fl*) allele. Primer-pairs used for genotyping are depicted with arrows. **(B)** Example
829 genotyping of the targeted allele and recombination events. Founder animal is in lane 2. The primer-
830 pairs shown in panel A were used. **(C)** OCA-B immunoblots from spleens of control, *fl/fl* and *Δ/Δ*
831 animals. BJA-B B cell nuclear extract is shown as a positive control (lane 1). **(D)** The *Ocab* (*Pou2af1*)
832 conditional allele was crossed to CD4-cre. Total splenic CD4$^+$ T cells were isolated from an
833 *Ocab*$^{fl/fl}$CD4-cre animal or a *Ocab*$^{+/fl}$CD4-cre littermate control, and stimulated for 2 d in vitro using
834 plate-bound CD3ε and soluble CD28 antibodies. An OCA-B immunoblot of stimulated total T cells is
835 shown. β-actin is shown as a loading control. **(E)** To generate NOD.*Ocab* conditional mice by speed
836 congenic backcross, microsatellite repeat polymorphisms at the *Idd* loci were tested by PCR using the
837 primers in Supplementary Table 1. Backcross generations 2 and 4 (B2 and B4) are shown (lanes 3 and
838 4), together with parent C57BL/6 (lane 1) and target NOD (lane 2) genomic DNA as controls. Images
839 are of different PCR products resolved using agarose or polyacrylamide gel electrophoresis. **(F)**
840 Example genotyping of *Ocab* wild-type and conditional alleles in B4 backcrossed mice. An agarose
841 gel image is shown. Mouse #122 corresponds to the B4 animal shown in B and was used as the
842 founder animal. This animal was crossed NOD.CD4-cre for subsequent experiments with the
843 conditional allele.
844
845 Figure S2. **Unaltered T cell populations and TCR representation in prediabetic**
846 **NOD.*Ocab*$^{fl/fl}$CD4-cre pancreatic lymph nodes compared to NOD.*Ocab*$^{fl/fl}$ littermate controls. (A)**
847 CD3$^+$ T cells were isolated and combined from the PLNs of three 8 week-old NOD.*Ocab*$^{fl/fl}$CD4-cre
848 mice or three NOD.*Ocab*$^{fl/fl}$ littermate controls. scRNAseq was performed. Clusters were overlaid in
849 UMAP plots. **(B)** Six different populations from A were analyzed for differential gene expression.
850 Identified genes are shown as scatter plots. Significantly differentially expressed genes (adjusted *p*-
851 value <0.05) are shown in red. **(C)** % contribution of individual Vb chains is shown. **(D)** *Trbv13-3*
852 expressing cells are shown in blue superimposed on the same UMAP scRNAseq data as in A. The
853 effector CD8$^+$ T cell cluster is highlighted in red.
854
855 Figure S3. **TCR beta chain representation across the entire population of prediabetic**
856 **NOD.*Ocab*$^{fl/fl}$CD4-cre pancreatic islets compared to NOD.*Ocab*$^{fl/fl}$ littermate controls.** Four 12
857 week-old mice in each group were combined for scRNAseq TCR analysis.

858

859 Figure S4. **Germline and T cell conditional OCA-B loss has no effect in two different T1D**
860 **transplant model systems. (A)** 5×10^5 purified $CD4^+CD62L^+Vb4^+$ T cells from NOD.BDC2.5.*Ocab*$^{-/-}$
861 or heterozygous control NOD.BDC2.5.*Ocab*$^{+/-}$ donors were injected retro-orbitally into NOD.SCID
862 recipients (n=7-8 per group). T1D-free survival following transplant is shown. **(B)** 10,000 OT-I T cells
863 were transferred retro-orbitally into C57BL6 RIP-mOVA;*Ocab*$^{fl/fl}$CD4-cre mice or littermate RIP-
864 mOVA;*Ocab*$^{fl/fl}$ controls. Mice were infected with 2000 cfu *Listeria monocytogenes* expressing
865 chicken ovalbumin (Lm-OVA) later the same day. Glucose was measured every two days and plotted.
866 Two mice in each group were used.

867

868 Figure S5. **Tat- but not OVA-conjugated peptides concentrate in cultured T cells.** $CD3^+$ T cells
869 were isolated from the spleens or pancreata of NOD mice and were incubated with 40 μM FITC-
870 conjugated OVA control peptide, or FITC-conjugated to the TAT membrane-penetrating peptide for
871 15 min. Cells with concentrated FITC fluorescence were observed by epifluorescence microscopy.
872 Images were taken at 40× magnification.

873

874 Table S1. **Loci for type 1 diabetes susceptibility and resistance in NOD/ShiLtJ mice, and**
875 **oligonucleotide primer-pairs used for PCR amplification of *Idd* loci microsatellite markers.**
876 Related to Supplemental Figure S1.

877

878 Table S2. **Gene expression comparisons in T cells taken from PLNs of 8 week-old**
879 **NOD.*Ocab*$^{fl/fl}$CD4-cre and NOD.*Ocab*$^{fl/fl}$ littermate controls.** Related to Supplemental Figure S2.

880

881 Table S3. **Expression levels of *Ccl1* mRNA in naïve, stimulated, rested and re-stimulated OCA-**
882 **B/Pou2af1-deficient T cells relative to controls.** Related to Figure 1.

883

884 Table S4. **Gene expression comparisons in total $CD45^+$ cells taken from pancreatic islets of 12**
885 **week-old prediabetic NOD.*Ocab*$^{fl/fl}$CD4-cre and NOD.*Ocab*$^{fl/fl}$ littermate controls.** Related to
886 Figure 2.

887 **References**

888 Antony-Debre, I., A. Paul, J. Leite, K. Mitchell, H.M. Kim, L.A. Carvajal, T.I. Todorova, K. Huang, A. Kumar, A.A.
889 Farahat, B. Bartholdy, S.R. Narayanagari, J. Chen, A. Ambesi-Impiombato, A.A. Ferrando, I. Mantzaris,
890 E. Gavathiotis, A. Verma, B. Will, D.W. Boykin, W.D. Wilson, G.M. Poon, and U. Steidl. 2017.
891 Pharmacological inhibition of the transcription factor PU.1 in leukemia. *J Clin Invest* 127:4297-4313.
892 Berry, G., and H. Waldner. 2013. Accelerated type 1 diabetes induction in mice by adoptive transfer of
893 diabetogenic CD4+ T cells. *J Vis Exp* e50389.
894 Cantor, J., and K. Haskins. 2007. Recruitment and activation of macrophages by pathogenic CD4 T cells in type
895 1 diabetes: evidence for involvement of CCR8 and CCL1. *J Immunol* 179:5760-5767.
896 Caron, N.J., S.P. Quenneville, and J.P. Tremblay. 2004. Endosome disruption enhances the functional nuclear
897 delivery of Tat-fusion proteins. *Biochem Biophys Res Commun* 319:12-20.
898 Carter, S., S. Miard, A. Caron, S. Sallé-Lefort, P. St-Pierre, F.F. Anhê, E. Lavoie-Charland, P. Blais-Lecours, M.C.
899 Drolet, J.S. Lefebvre, J. Lacombe, Y. Deshaies, J. Couet, M. Laplante, M. Ferron, Y. Bossé, A. Marette, D.
900 Richard, D. Marsolais, and F. Picard. 2018. Loss of OcaB Prevents Age-Induced Fat Accretion and Insulin
901 Resistance by Altering B-Lymphocyte Transition and Promoting Energy Expenditure. *Diabetes* 67:1285-
902 1296.
903 Casellas, R., M. Jankovic, G. Meyer, A. Gazumyan, Y. Luo, R. Roeder, and M. Nussenzweig. 2002. OcaB is
904 required for normal transcription and V(D)J recombination of a subset of immunoglobulin kappa
905 genes. *Cell* 110:575-585.
906 Chai, J.G., and R.I. Lechler. 1997. Immobilized anti-CD3 mAb induces anergy in murine naive and memory CD4+
907 T cells in vitro. *Int Immunol* 9:935-944.
908 Chasman, D., K. Cepek, P.A. Sharp, and C.O. Pabo. 1999. Crystal structure of an OCA-B peptide bound to an
909 Oct-1 POU domain/octamer DNA complex: specific recognition of a protein-DNA interface. *Genes Dev*
910 13:2650-2657.
911 Chee, J., H.J. Ko, A. Skowera, G. Jhala, T. Catterall, K.L. Graham, R.M. Sutherland, H.E. Thomas, A.M. Lew, M.
912 Peakman, T.W. Kay, and B. Krishnamurthy. 2014. Effector-memory T cells develop in islets and report
913 islet pathology in type 1 diabetes. *J Immunol* 192:572-580.
914 Chevrier, S., T. Kratina, D. Emslie, A. Karnowski, and L.M. Corcoran. 2014. Germinal center-independent, IgM-
915 mediated autoimmunity in sanroque mice lacking Obf1. *Immunol Cell Biol* 92:12-19.
916 Citro, A., A. Valle, E. Cantarelli, A. Mercalli, S. Pellegrini, D. Liberati, L. Daffonchio, O. Kastsiuchenka, P.A.
917 Ruffini, M. Battaglia, M. Allegretti, and L. Piemonti. 2015. CXCR1/2 inhibition blocks and reverses type
918 1 diabetes in mice. *Diabetes* 64:1329-1340.
919 Cooke, D.W., and L. Plotnick. 2008. Type 1 diabetes mellitus in pediatrics. *Pediatr Rev* 29:374-384; quiz 385.
920 Cunninghame Graham, D.S., A.K. Wong, N.J. McHugh, J.C. Whittaker, and T.J. Vyse. 2006. Evidence for unique
921 association signals in SLE at the CD28-CTLA4-ICOS locus in a family-based study. *Hum Mol Genet*
922 15:3195-3205.
923 Delong, T., T.A. Wiles, R.L. Baker, B. Bradley, G. Barbour, R. Reisdorph, M. Armstrong, R.L. Powell, N. Reisdorph,
924 N. Kumar, C.M. Elso, M. DeNicola, R. Bottino, A.C. Powers, D.M. Harlan, S.C. Kent, S.I. Mannering, and
925 K. Haskins. 2016. Pathogenic CD4 T cells in type 1 diabetes recognize epitopes formed by peptide
926 fusion. *Science* 351:711-714.
927 Diana, J., and A. Lehuen. 2014. Macrophages and beta-cells are responsible for CXCR2-mediated neutrophil
928 infiltration of the pancreas during autoimmune diabetes. *EMBO Mol Med* 6:1090-1104.
929 Dong, C., A.E. Juedes, U.A. Temann, S. Shresta, J.P. Allison, N.H. Ruddle, and R.A. Flavell. 2001. ICOS co-
930 stimulatory receptor is essential for T-cell activation and function. *Nature* 409:97-101.
931 Dong, C., and R.I. Nurieva. 2003. Regulation of immune and autoimmune responses by ICOS. *J Autoimmun*
932 21:255-260.
933 Farh, K.K., A. Marson, J. Zhu, M. Kleinewietfeld, W.J. Housley, S. Beik, N. Shoresh, H. Whitton, R.J. Ryan, A.A.
934 Shishkin, M. Hatan, M.J. Carrasco-Alfonso, D. Mayer, C.J. Luckey, N.A. Patsopoulos, P.L. De Jager, V.K.

935 Kuchroo, C.B. Epstein, M.J. Daly, D.A. Hafler, and B.E. Bernstein. 2015. Genetic and epigenetic fine
936 mapping of causal autoimmune disease variants. *Nature* 518:337-343.
937 Games Collaborative, G., M. Ban, D. Booth, R. Heard, G. Stewart, A. Goris, K. Vandenbroeck, B. Dubois, M.
938 Laaksonen, J. Ilonen, M. Alizadeh, G. Edan, M.C. Babron, D. Brassat, M. Clanet, I. Cournu-Rebeix, B.
939 Fontaine, G. Semana, R. Goedde, J. Epplen, A. Weber, C. Infante-Duarte, F. Zipp, C. Rajda, K. Bencsik, L.
940 Vecsei, S. Heggarty, C. Graham, S. Hawkins, M. Liguori, P. Momigliano-Richiardi, D. Caputo, L.M.
941 Grimaldi, M. Leone, L. Massacesi, C. Milanese, M. Salvetti, G. Savettieri, M. Trojano, B. Bielecki, M.P.
942 Mycko, K. Selmaj, M. Santos, P. Maciel, C. Pereira, A. Silva, B.M. Silva, F. Coraddu, M.G. Marrosu, E.
943 Akesson, J. Hillert, P. Datta, A. Oturai, H.F. Harbo, A. Spurkland, R. Goertsches, P. Villoslada, M.
944 Eraksoy, A. Hensiek, A. Compston, E. Setakis, J. Gray, T.W. Yeo, and S. Sawcer. 2006. Linkage
945 disequilibrium screening for multiple sclerosis implicates JAG1 and POU2AF1 as susceptibility genes in
946 Europeans. *J Neuroimmunol* 179:108-116.
947 Green, D.R. 2016. A BH3 Mimetic for Killing Cancer Cells. *Cell* 165:1560.
948 Gstaiger, M., O. Georgiev, H. van Leeuwen, P. van der Vliet, and W. Schaffner. 1996. The B cell coactivator
949 Bob1 shows DNA sequence-dependent complex formation with Oct-1/Oct-2 factors, leading to
950 differential promoter activation. *EMBO J* 15:2781-2790.
951 Gstaiger, M., L. Knoepfel, O. Georgiev, W. Schaffner, and C.M. Hovens. 1995. A B-cell coactivator of octamer-
952 binding transcription factors. *Nature* 373:360-362.
953 Haskins, K. 2005. Pathogenic T-cell clones in autoimmune diabetes: more lessons from the NOD mouse. *Adv*
954 *Immunol* 87:123-162.
955 Hattori, M., J.B. Buse, R.A. Jackson, L. Glimcher, M.E. Dorf, M. Minami, S. Makino, K. Moriwaki, H. Kuzuya, H.
956 Imura, and et al. 1986. The NOD mouse: recessive diabetogenic gene in the major histocompatibility
957 complex. *Science* 231:733-735.
958 Heng, T.S., M.W. Painter, and C. Immunological Genome Project. 2008. The Immunological Genome Project:
959 networks of gene expression in immune cells. *Nat Immunol* 9:1091-1094.
960 Ikegami, I., H. Takaki, S. Kamiya, R. Kamekura, and S. Ichimiya. 2019. Bob1 enhances RORgammat-mediated IL-
961 17A expression in Th17cells through interaction with RORgammat. *Biochem Biophys Res Commun*
962 514:1167-1171.
963 Kalekar, L.A., S.E. Schmiel, S.L. Nandiwada, W.Y. Lam, L.O. Barsness, N. Zhang, G.L. Stritesky, D. Malhotra, K.E.
964 Pauken, J.L. Linehan, M.G. O'Sullivan, B.T. Fife, K.A. Hogquist, M.K. Jenkins, and D.L. Mueller. 2016.
965 CD4(+) T cell anergy prevents autoimmunity and generates regulatory T cell precursors. *Nat Immunol*
966 17:304-314.
967 Katz, J.D., B. Wang, K. Haskins, C. Benoist, and D. Mathis. 1993. Following a diabetogenic T cell from genesis
968 through pathogenesis. *Cell* 74:1089-1100.
969 Kawakami, N., F. Odoardi, T. Ziemssen, M. Bradl, T. Ritter, O. Neuhaus, H. Lassmann, H. Wekerle, and A. Flugel.
970 2005. Autoimmune CD4+ T cell memory: lifelong persistence of encephalitogenic T cell clones in
971 healthy immune repertoires. *J Immunol* 175:69-81.
972 Kearney, E.R., K.A. Pape, D.Y. Loh, and M.K. Jenkins. 1994. Visualization of peptide-specific T cell immunity and
973 peripheral tolerance induction in vivo. *Immunity* 1:327-339.
974 Kiesler, P., A. Shakya, D. Tantin, and D. Vercelli. 2009. An allergy-associated polymorphism in a novel regulatory
975 element enhances IL13 expression. *Hum Mol Genet* 18:4513-4520.
976 Kim, H., L. Dickey, C. Stone, J.L. Jafek, T.E. Lane, and D. Tantin. 2019. T cell-selective deletion of Oct1 protects
977 animals from autoimmune neuroinflammation while maintaining neurotropic pathogen response. *J*
978 *Neuroinflammation* 16:133.
979 Kim, U., X.F. Qin, S. Gong, S. Stevens, Y. Luo, M. Nussenzweig, and R.G. Roeder. 1996. The B-cell-specific
980 transcription coactivator OCA-B/OBF-1/Bob-1 is essential for normal production of immunoglobulin
981 isotypes. *Nature* 383:542-547.
982 Klemm, J.D., M.A. Rould, R. Aurora, W. Herr, and C.O. Pabo. 1994. Crystal structure of the Oct-1 POU domain
983 bound to an octamer site: DNA recognition with tethered DNA-binding modules. *Cell* 77:21-32.

984 Krautwald, S., E. Ziegler, K. Tiede, R. Pust, and U. Kunzendorf. 2004. Transduction of the TAT-FLIP fusion
985 protein results in transient resistance to Fas-induced apoptosis in vivo. *The Journal of biological*
986 *chemistry* 279:44005-44011.
987 Krishnamurthy, B., L. Mariana, S.A. Gellert, P.G. Colman, L.C. Harrison, A.M. Lew, P. Santamaria, H.E. Thomas,
988 and T.W. Kay. 2008. Autoimmunity to both proinsulin and IGRP is required for diabetes in nonobese
989 diabetic 8.3 TCR transgenic mice. *J Immunol* 180:4458-4464.
990 Kurts, C., F.R. Carbone, M. Barnden, E. Blanas, J. Allison, W.R. Heath, and J.F. Miller. 1997. CD4+ T cell help
991 impairs CD8+ T cell deletion induced by cross-presentation of self-antigens and favors autoimmunity. *J*
992 *Exp Med* 186:2057-2062.
993 Kurts, C., W.R. Heath, F.R. Carbone, J. Allison, J.F. Miller, and H. Kosaka. 1996. Constitutive class I-restricted
994 exogenous presentation of self antigens in vivo. *J Exp Med* 184:923-930.
995 Leon Rodriguez, D.A., F.D. Carmona, L.E. Echeverria, C.I. Gonzalez, and J. Martin. 2016. IL18 Gene Variants
996 Influence the Susceptibility to Chagas Disease. *PLoS Negl Trop Dis* 10:e0004583.
997 Lernmark, A., and H.E. Larsson. 2013. Immune therapy in type 1 diabetes mellitus. *Nat Rev Endocrinol* 9:92-
998 103.
999 Li, L., Q. He, A. Garland, Z. Yi, L.T. Aybar, T.B. Kepler, J.A. Frelinger, B. Wang, and R. Tisch. 2009. beta cell-
1000 specific CD4+ T cell clonotypes in peripheral blood and the pancreatic islets are distinct. *J Immunol*
1001 183:7585-7591.
1002 Makino, S., Y. Muraoka, Y. Kishimoto, and Y. Hayashi. 1985. Genetic analysis for insulitis in NOD mice. *Jikken*
1003 *Dobutsu* 34:425-431.
1004 Martinez, R.J., N. Zhang, S.R. Thomas, S.L. Nandiwada, M.K. Jenkins, B.A. Binstadt, and D.L. Mueller. 2012.
1005 Arthritogenic self-reactive CD4+ T cells acquire an FR4hiCD73hi anergic state in the presence of Foxp3+
1006 regulatory T cells. *J Immunol* 188:170-181.
1007 Maurano, M.T., R. Humbert, E. Rynes, R.E. Thurman, E. Haugen, H. Wang, A.P. Reynolds, R. Sandstrom, H. Qu,
1008 J. Brody, A. Shafer, F. Neri, K. Lee, T. Kutyavin, S. Stehling-Sun, A.K. Johnson, T.K. Canfield, E. Giste, M.
1009 Diegel, D. Bates, R.S. Hansen, S. Neph, P.J. Sabo, S. Heimfeld, A. Raubitschek, S. Ziegler, C. Cotsapas, N.
1010 Sotoodehnia, I. Glass, S.R. Sunyaev, R. Kaul, and J.A. Stamatoyannopoulos. 2012. Systematic
1011 localization of common disease-associated variation in regulatory DNA. *Science* 337:1190-1195.
1012 Nakamura, M., N. Nishida, M. Kawashima, Y. Aiba, A. Tanaka, M. Yasunami, H. Nakamura, A. Komori, M.
1013 Nakamuta, M. Zeniya, E. Hashimoto, H. Ohira, K. Yamamoto, M. Onji, S. Kaneko, M. Honda, S.
1014 Yamagiwa, K. Nakao, T. Ichida, H. Takikawa, M. Seike, T. Umemura, Y. Ueno, S. Sakisaka, K. Kikuchi, H.
1015 Ebinuma, N. Yamashiki, S. Tamura, Y. Sugawara, A. Mori, S. Yagi, K. Shirabe, A. Taketomi, K. Arai, K.
1016 Monoe, T. Ichikawa, M. Taniai, Y. Miyake, T. Kumagi, M. Abe, K. Yoshizawa, S. Joshita, S. Shimoda, K.
1017 Honda, H. Takahashi, K. Hirano, Y. Takeyama, K. Harada, K. Migita, M. Ito, H. Yatsuhashi, N. Fukushima,
1018 H. Ota, T. Komatsu, T. Saoshiro, J. Ishida, H. Kouno, H. Kouno, M. Yagura, M. Kobayashi, T. Muro, N.
1019 Masaki, K. Hirata, Y. Watanabe, Y. Nakamura, M. Shimada, N. Hirashima, T. Komeda, K. Sugi, M. Koga,
1020 K. Ario, E. Takesaki, Y. Maehara, S. Uemoto, N. Kokudo, H. Tsubouchi, M. Mizokami, Y. Nakanuma, K.
1021 Tokunaga, and H. Ishibashi. 2012. Genome-wide association study identifies TNFSF15 and POU2AF1 as
1022 susceptibility loci for primary biliary cirrhosis in the Japanese population. *Am J Hum Genet* 91:721-728.
1023 Newby, B.N., T.M. Brusko, B. Zou, M.A. Atkinson, M. Clare-Salzler, and C.E. Mathews. 2017. Type 1 Interferons
1024 Potentiate Human CD8(+) T-Cell Cytotoxicity Through a STAT4- and Granzyme B-Dependent Pathway.
1025 *Diabetes* 66:3061-3071.
1026 Parker, M.J., S. Xue, J.J. Alexander, C.H. Wasserfall, M.L. Campbell-Thompson, M. Battaglia, S. Gregori, C.E.
1027 Mathews, S. Song, M. Troutt, S. Eisenbeis, J. Williams, D.A. Schatz, M.J. Haller, and M.A. Atkinson.
1028 2009. Immune depletion with cellular mobilization imparts immunoregulation and reverses
1029 autoimmune diabetes in nonobese diabetic mice. *Diabetes* 58:2277-2284.
1030 Peterson, J.D., R. Berg, J.D. Piganelli, M. Poulin, and K. Haskins. 1998. Analysis of leukocytes recruited to the
1031 pancreas by diabetogenic T cell clones. *Cell Immunol* 189:92-98.

1032 Polo, J.M., T. Dell'Oso, S.M. Ranuncolo, L. Cerchietti, D. Beck, G.F. Da Silva, G.G. Prive, J.D. Licht, and A.
1033 Melnick. 2004. Specific peptide interference reveals BCL6 transcriptional and oncogenic mechanisms in
1034 B-cell lymphoma cells. *Nat Med* 10:1329-1335.
1035 Presa, M., Y.G. Chen, A.E. Grier, E.H. Leiter, M.A. Brehm, D.L. Greiner, L.D. Shultz, and D.V. Serreze. 2015. The
1036 Presence and Preferential Activation of Regulatory T Cells Diminish Adoptive Transfer of Autoimmune
1037 Diabetes by Polyclonal Nonobese Diabetic (NOD) T Cell Effectors into NSG versus NOD-scid Mice. *J*
1038 *Immunol* 195:3011-3019.
1039 Qin, X.F., A. Reichlin, Y. Luo, R.G. Roeder, and M.C. Nussenzweig. 1998. OCA-B integrates B cell antigen
1040 receptor-, CD40L- and IL 4-mediated signals for the germinal center pathway of B cell development.
1041 *EMBO J* 17:5066-5075.
1042 Rosmalen, J.G., T. Martin, C. Dobbs, J.S. Voerman, H.A. Drexhage, K. Haskins, and P.J. Leenen. 2000. Subsets of
1043 macrophages and dendritic cells in nonobese diabetic mouse pancreatic inflammatory infiltrates:
1044 correlation with the development of diabetes. *Lab Invest* 80:23-30.
1045 Schloot, N.C., P. Hanifi-Moghaddam, C. Goebel, S.V. Shatavi, S. Flohe, H. Kolb, and H. Rothe. 2002. Serum IFN-
1046 gamma and IL-10 levels are associated with disease progression in non-obese diabetic mice. *Diabetes*
1047 *Metab Res Rev* 18:64-70.
1048 Schwarze, S.R., K.A. Hruska, and S.F. Dowdy. 2000. Protein transduction: unrestricted delivery into all cells?
1049 *Trends Cell Biol* 10:290-295.
1050 Serreze, D.V., M. Bridgett, H.D. Chapman, E. Chen, S.D. Richard, and E.H. Leiter. 1998. Subcongenic analysis of
1051 the Idd13 locus in NOD/Lt mice: evidence for several susceptibility genes including a possible
1052 diabetogenic role for beta 2-microglobulin. *J Immunol* 160:1472-1478.
1053 Serreze, D.V., H.D. Chapman, D.S. Varnum, M.S. Hanson, P.C. Reifsnyder, S.D. Richard, S.A. Fleming, E.H. Leiter,
1054 and L.D. Shultz. 1996. B lymphocytes are essential for the initiation of T cell-mediated autoimmune
1055 diabetes: analysis of a new "speed congenic" stock of NOD.Ig mu null mice. *J Exp Med* 184:2049-2053.
1056 Shakya, A., A. Goren, A. Shalek, C.N. German, J. Snook, V.K. Kuchroo, N. Yosef, R.C. Chan, A. Regev, M.A.
1057 Williams, and D. Tantin. 2015. Oct1 and OCA-B are selectively required for CD4 memory T cell function.
1058 *J Exp Med* 212:2115-2131.
1059 Shakya, A., J. Kang, J. Chumley, M.A. Williams, and D. Tantin. 2011. Oct1 is a switchable, bipotential stabilizer
1060 of repressed and inducible transcriptional states. *The Journal of biological chemistry* 286:450-459.
1061 Shi, W., Y. Liao, S.N. Willis, N. Taubenheim, M. Inouye, D.M. Tarlinton, G.K. Smyth, P.D. Hodgkin, S.L. Nutt, and
1062 L.M. Corcoran. 2015. Transcriptional profiling of mouse B cell terminal differentiation defines a
1063 signature for antibody-secreting plasma cells. *Nat Immunol* 16:663-673.
1064 Sitrin, J., A. Ring, K.C. Garcia, C. Benoist, and D. Mathis. 2013. Regulatory T cells control NK cells in an insulitic
1065 lesion by depriving them of IL-2. *J Exp Med* 210:1153-1165.
1066 Skwarczynska, M., and C. Ottmann. 2015. Protein-protein interactions as drug targets. *Future Med Chem*
1067 7:2195-2219.
1068 Staeva, T.P., L. Chatenoud, R. Insel, and M.A. Atkinson. 2013. Recent lessons learned from prevention and
1069 recent-onset type 1 diabetes immunotherapy trials. *Diabetes* 62:9-17.
1070 Sun, J., G. Matthias, M.J. Mihatsch, K. Georgopoulos, and P. Matthias. 2003. Lack of the transcriptional
1071 coactivator OBF-1 prevents the development of systemic lupus erythematosus-like phenotypes in
1072 Aiolos mutant mice. *J Immunol* 170:1699-1706.
1073 Testa, G., J. Schaft, F. van der Hoeven, S. Glaser, K. Anastassiadis, Y. Zhang, T. Hermann, W. Stremmel, and A.F.
1074 Stewart. 2004. A reliable lacZ expression reporter cassette for multipurpose, knockout-first alleles.
1075 *Genesis* 38:151-158.
1076 Thin, T.H., E. Kim, S. Yeh, E.R. Sampson, Y.T. Chen, L.L. Collins, R. Basavappa, and C. Chang. 2002. Mutations in
1077 the helix 3 region of the androgen receptor abrogate ARA70 promotion of 17beta-estradiol-induced
1078 androgen receptor transactivation. *The Journal of biological chemistry* 277:36499-36508.
1079 Tuettenberg, A., E. Huter, M. Hubo, J. Horn, J. Knop, B. Grimbacher, R.A. Kroczek, S. Stoll, and H. Jonuleit. 2009.
1080 The role of ICOS in directing T cell responses: ICOS-dependent induction of T cell anergy by tolerogenic
1081 dendritic cells. *J Immunol* 182:3349-3356.

1082 Van Belle, T.L., P. Taylor, and M.G. von Herrath. 2009. Mouse Models for Type 1 Diabetes. *Drug Discov Today*
1083 *Dis Models* 6:41-45.
1084 van Heel, D.A., I.A. Udalova, A.P. De Silva, D.P. McGovern, Y. Kinouchi, J. Hull, N.J. Lench, L.R. Cardon, A.H.
1085 Carey, D.P. Jewell, and D. Kwiatkowski. 2002. Inflammatory bowel disease is associated with a TNF
1086 polymorphism that affects an interaction between the OCT1 and NF(-kappa)B transcription factors.
1087 *Hum Mol Genet* 11:1281-1289.
1088 Vanasek, T.L., A. Khoruts, T. Zell, and D.L. Mueller. 2001. Antagonistic roles for CTLA-4 and the mammalian
1089 target of rapamycin in the regulation of clonal anergy: enhanced cell cycle progression promotes recall
1090 antigen responsiveness. *J Immunol* 167:5636-5644.
1091 Verdaguer, J., D. Schmidt, A. Amrani, B. Anderson, N. Averill, and P. Santamaria. 1997. Spontaneous
1092 autoimmune diabetes in monoclonal T cell nonobese diabetic mice. *J Exp Med* 186:1663-1676.
1093 Vince, N., H. Li, V. Ramsuran, V. Naranbhai, F.M. Duh, B.P. Fairfax, B. Saleh, J.C. Knight, S.K. Anderson, and M.
1094 Carrington. 2016. HLA-C Level Is Regulated by a Polymorphic Oct1 Binding Site in the HLA-C Promoter
1095 Region. *Am J Hum Genet* 99:1353-1358.
1096 Wang, B., I. Andre, A. Gonzalez, J.D. Katz, M. Aguet, C. Benoist, and D. Mathis. 1997. Interferon-gamma
1097 impacts at multiple points during the progression of autoimmune diabetes. *Proc Natl Acad Sci U S A*
1098 94:13844-13849.
1099 Wong, C.P., L. Li, J.A. Frelinger, and R. Tisch. 2006. Early autoimmune destruction of islet grafts is associated
1100 with a restricted repertoire of IGRP-specific CD8+ T cells in diabetic nonobese diabetic mice. *J Immunol*
1101 176:1637-1644.
1102 Yamane, K., C. Toumazou, Y. Tsukada, H. Erdjument-Bromage, P. Tempst, J. Wong, and Y. Zhang. 2006.
1103 JHDM2A, a JmjC-containing H3K9 demethylase, facilitates transcription activation by androgen
1104 receptor. *Cell* 125:483-495.
1105 Yeo, L., A. Woodwyk, S. Sood, A. Lorenc, M. Eichmann, I. Pujol-Autonell, R. Melchiotti, A. Skowera, E. Fidanis,
1106 G.M. Dolton, K. Tungatt, A.K. Sewell, S. Heck, A. Saxena, C.A. Beam, and M. Peakman. 2018.
1107 Autoreactive T effector memory differentiation mirrors beta cell function in type 1 diabetes. *J Clin*
1108 *Invest* 128:3460-3474.
1109 Yosef, N., A.K. Shalek, J.T. Gaublomme, H. Jin, Y. Lee, A. Awasthi, C. Wu, K. Karwacz, S. Xiao, M. Jorgolli, D.
1110 Gennert, R. Satija, A. Shakya, D.Y. Lu, J.J. Trombetta, M.R. Pillai, P.J. Ratcliffe, M.L. Coleman, M. Bix, D.
1111 Tantin, H. Park, V.K. Kuchroo, and A. Regev. 2013. Dynamic regulatory network controlling TH17 cell
1112 differentiation. *Nature* 496:461-468.
1113 Zhang, C., I. Todorov, C.L. Lin, M. Atkinson, F. Kandeel, S. Forman, and D. Zeng. 2007. Elimination of insulitis
1114 and augmentation of islet beta cell regeneration via induction of chimerism in overtly diabetic NOD
1115 mice. *Proc Natl Acad Sci U S A* 104:2337-2342.
1116 Zuber, J., J. Shi, E. Wang, A.R. Rappaport, H. Herrmann, E.A. Sison, D. Magoon, J. Qi, K. Blatt, M. Wunderlich,
1117 M.J. Taylor, C. Johns, A. Chicas, J.C. Mulloy, S.C. Kogan, P. Brown, P. Valent, J.E. Bradner, S.W. Lowe,
1118 and C.R. Vakoc. 2011. RNAi screen identifies Brd4 as a therapeutic target in acute myeloid leukaemia.
1119 *Nature* 478:524-528.
1120 Zwilling, S., A. Dieckmann, P. Pfisterer, P. Angel, and T. Wirth. 1997. Inducible expression and phosphorylation
1121 of coactivator BOB.1/OBF.1 in T cells. *Science* 277:221-225.

1122

Kim et al. Figure 1

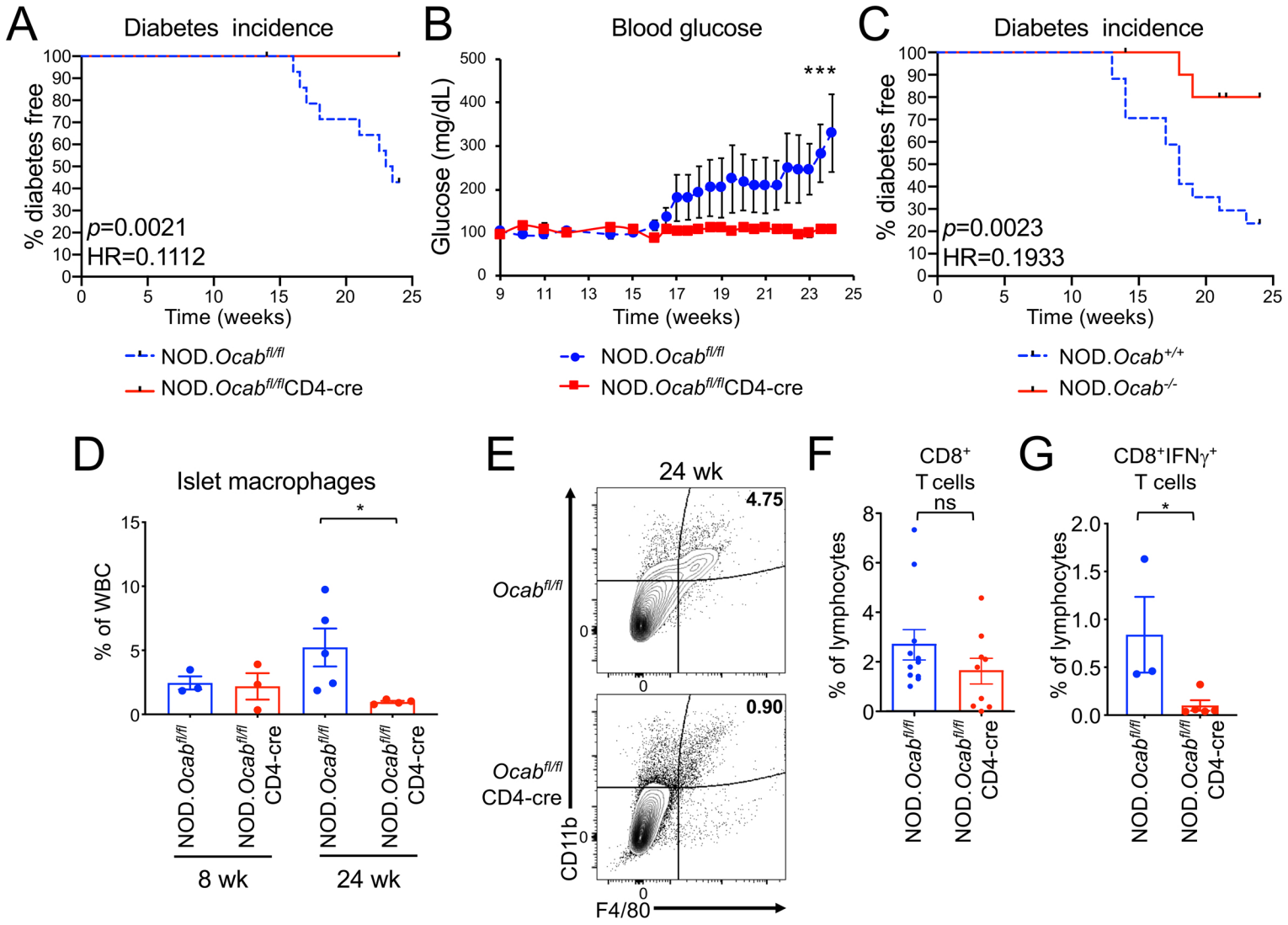

Kim et al. Figure 2

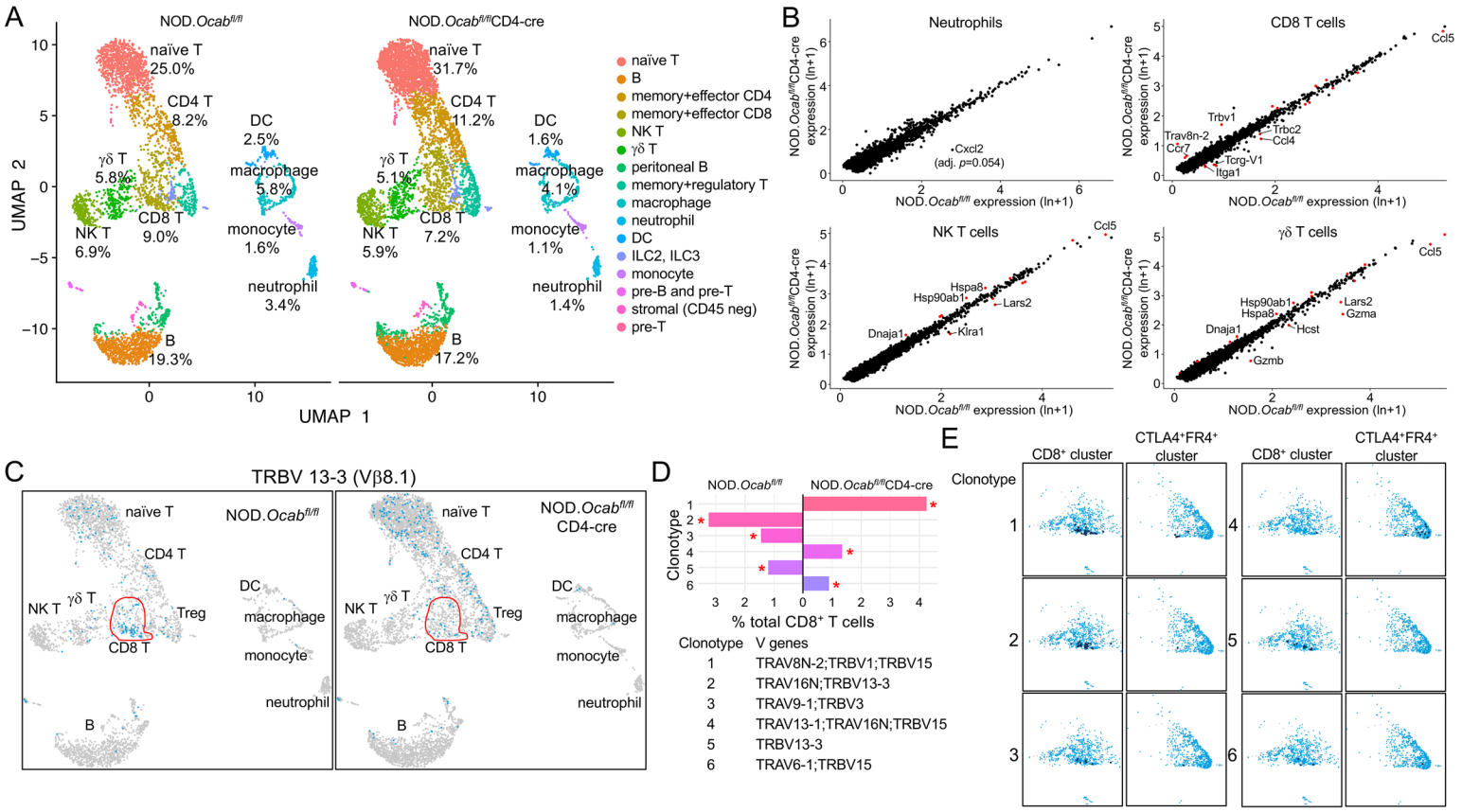

Kim et al. Figure 3

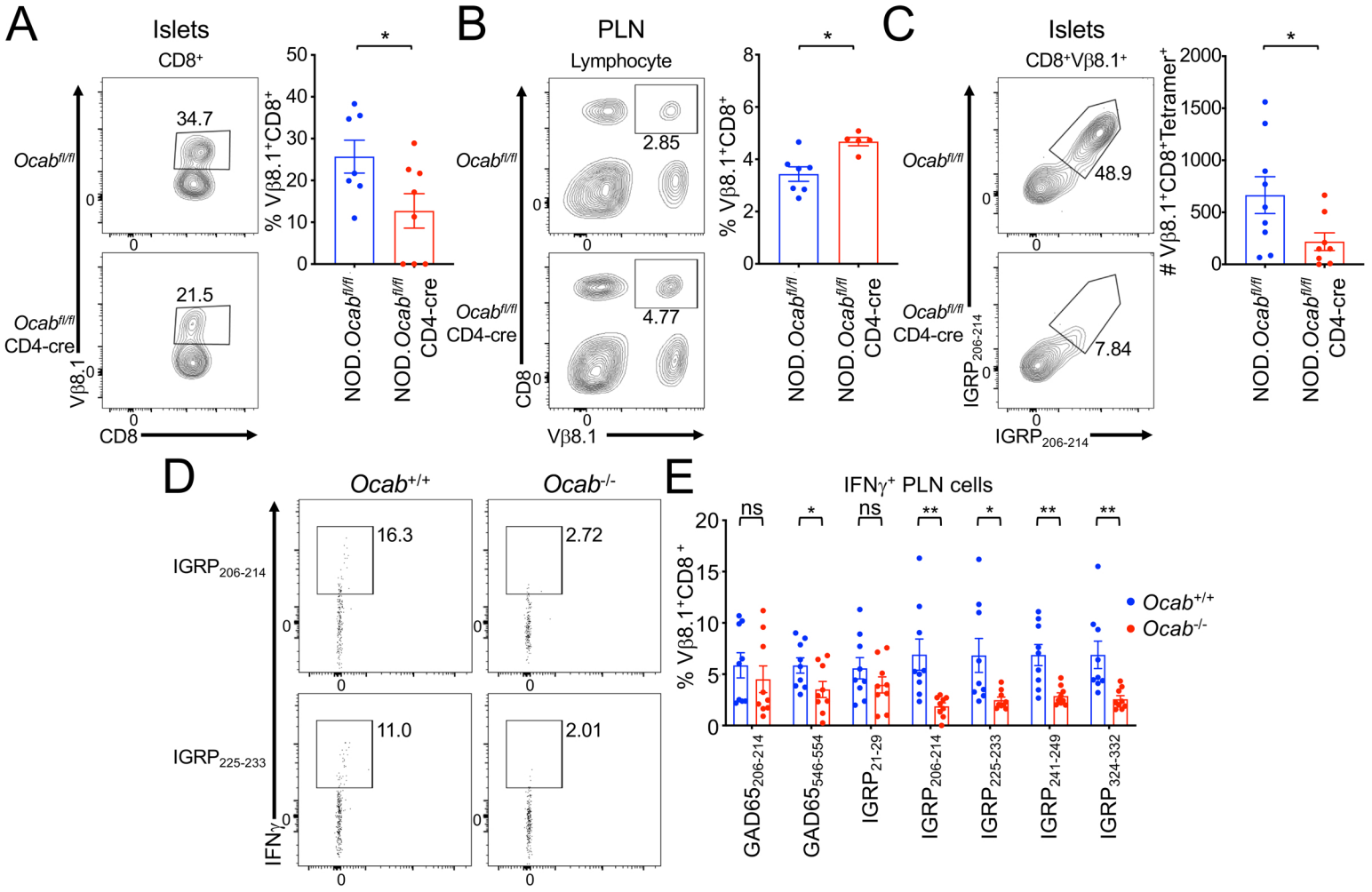

Kim et al. Figure 4

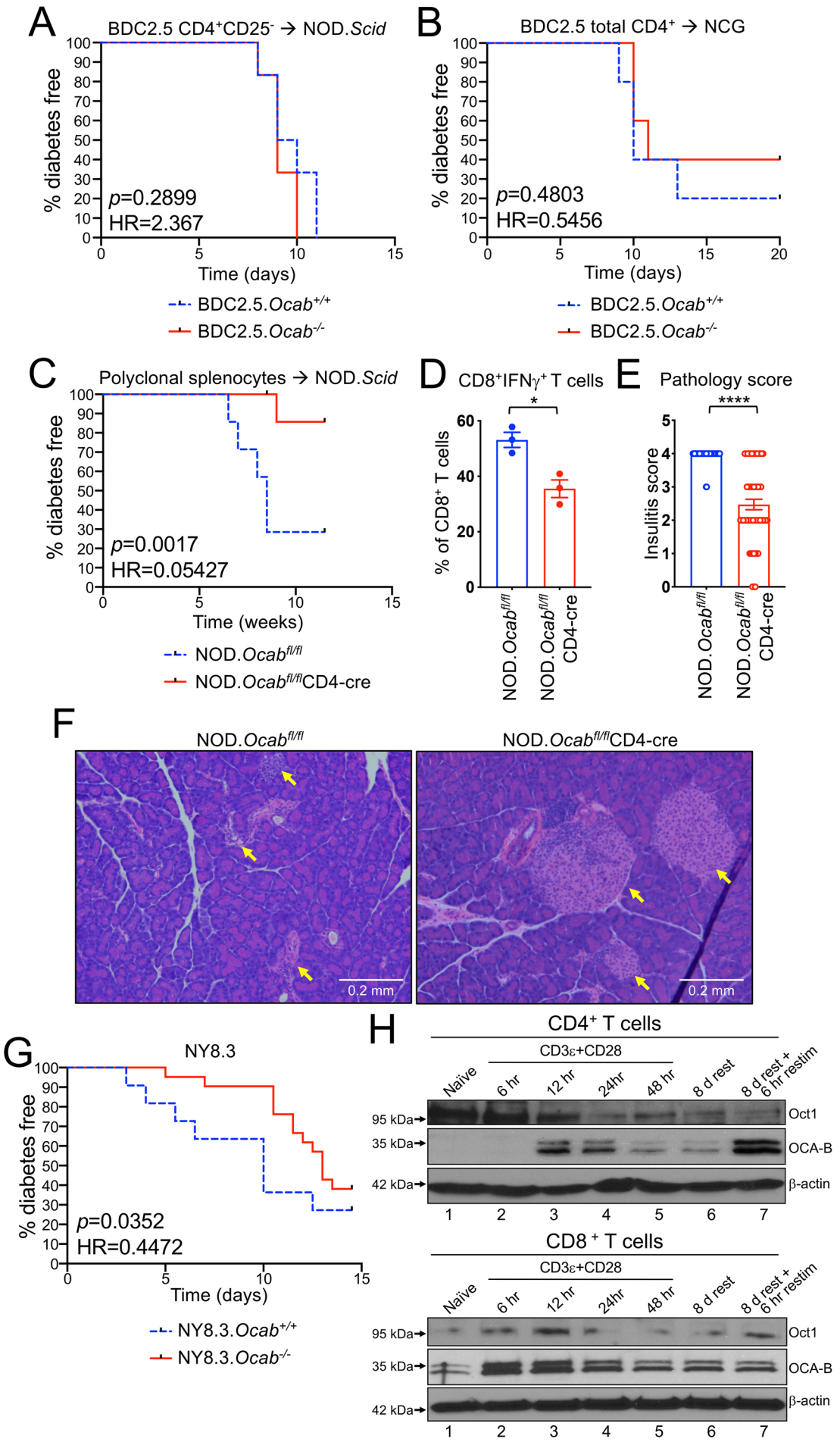

Kim et al. Figure 5

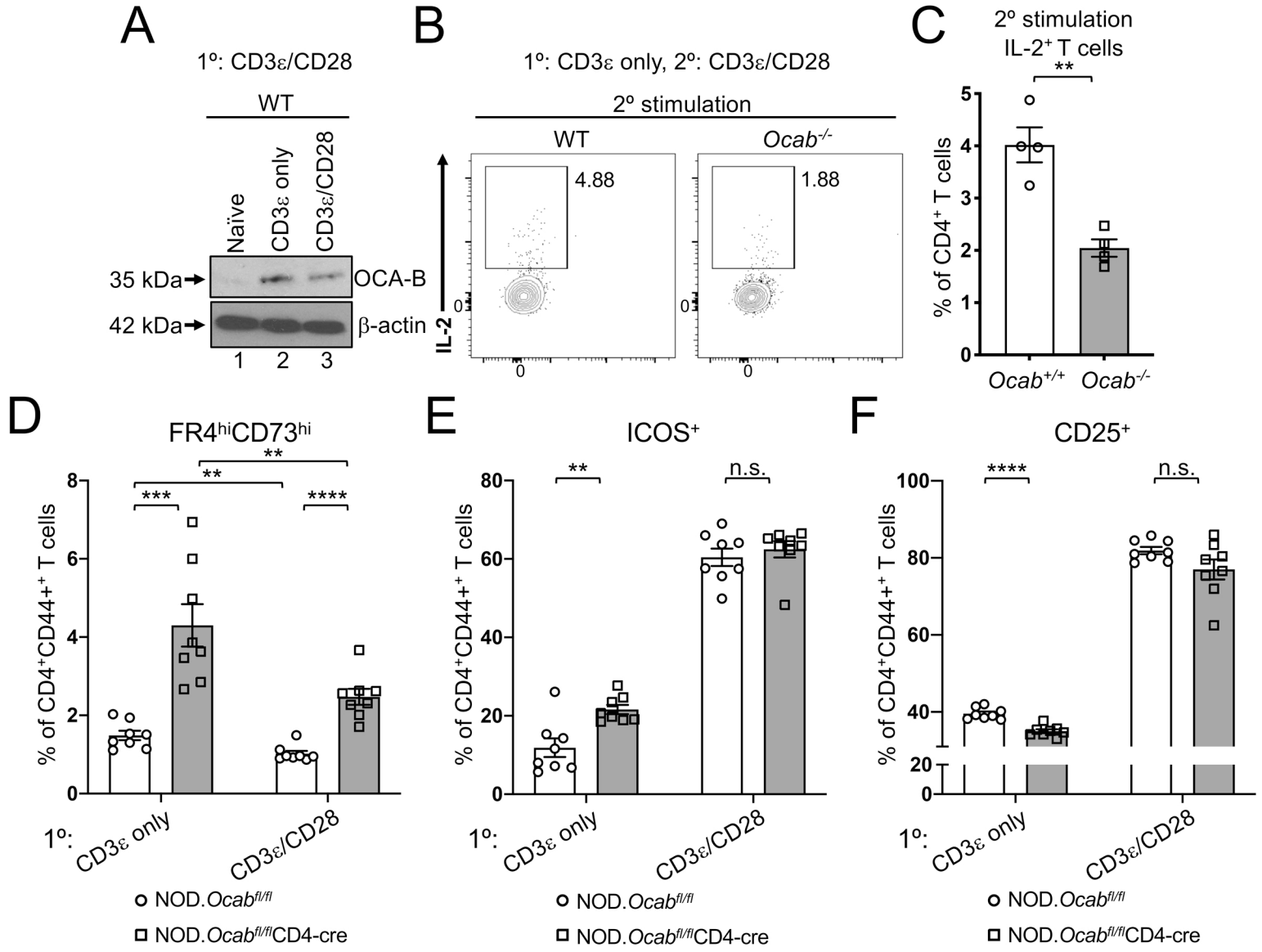

Kim et al. Figure 6

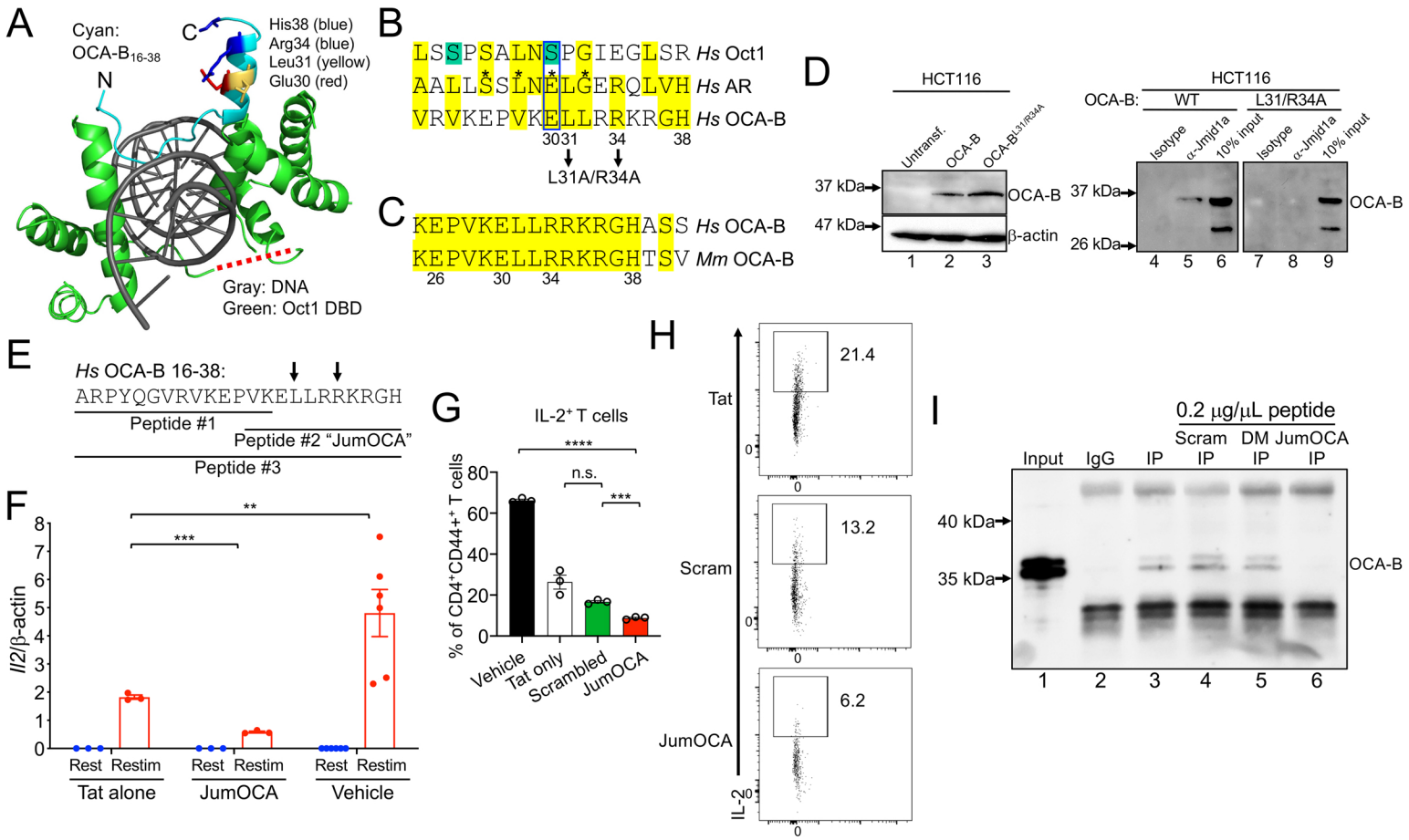
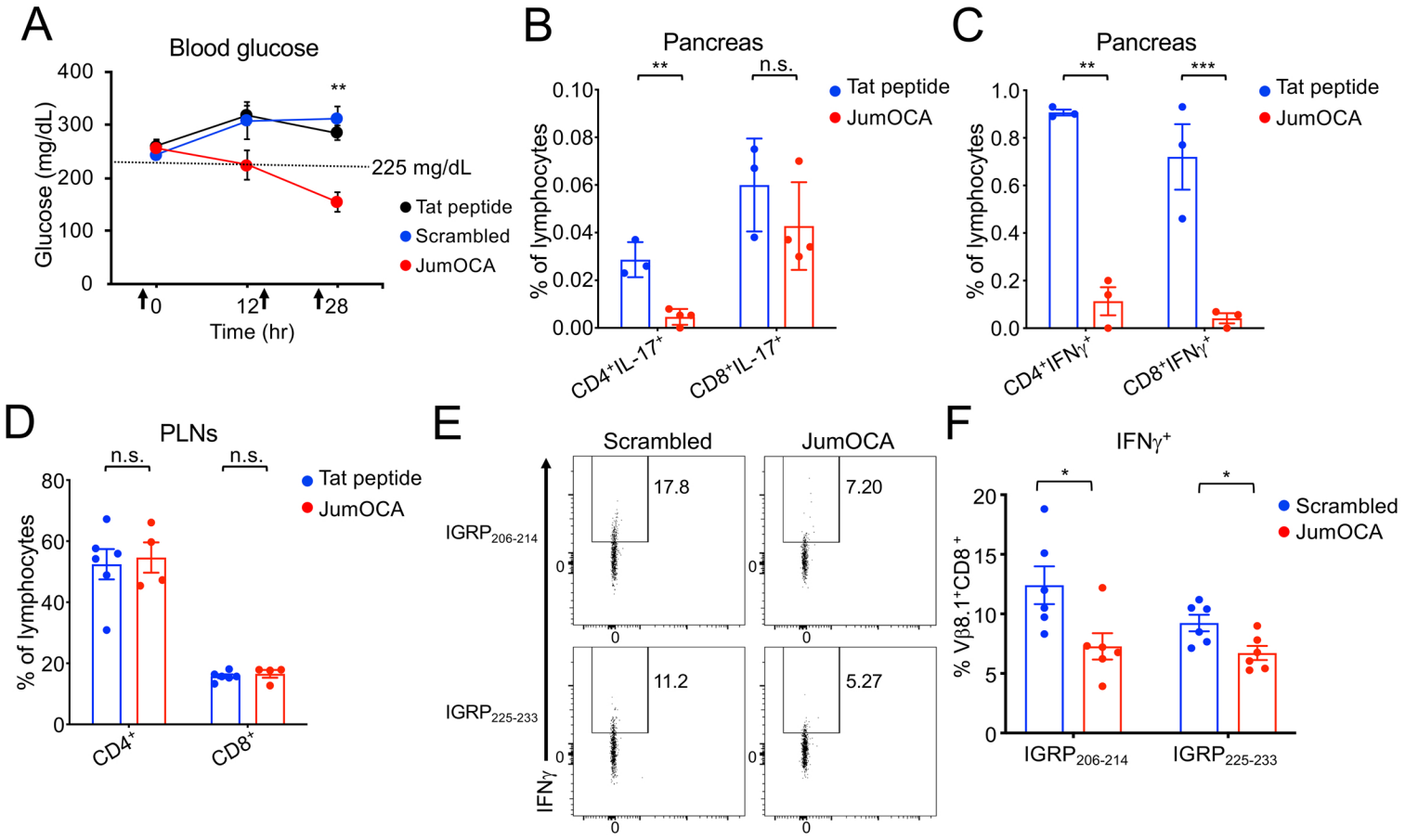
Kim et al. Figure 7